Tunable and abrupt thermal quenching of photoluminescence in high-resistivity Zn-doped GaN

Michael A. Reshchikov*
Department of Physics, Virginia Commonwealth University, Richmond, Virginia 23284-2000, USA

Alexander A. Kvasov†
Department of Physics, Virginia Commonwealth University, Richmond, Virginia 23284-2000, USA and
Department of Physics, St. Petersburg State University, St. Petersburg 199034, Russia

Marilyn F. Bishop and Tom McMullen
Department of Physics, Virginia Commonwealth University, Richmond, Virginia 23284-2000, USA and
Center for the Study of Biological Complexity, Virginia Commonwealth University, Richmond, Virginia 23284-2000, USA

Alexander Usikov, Vitali Soukhoveev, and Vladimir A. Dmitriev‡
Oxford Instruments TDI, Silver Spring, Maryland, USA

(Received 3 September 2010; revised manuscript received 4 April 2011; published 15 August 2011)

Tunable and abrupt thermal quenching of photoluminescence by increasing temperature has been observed for the blue band in high-resistivity Zn-doped GaN. The photoluminescence intensity dropped by several orders of magnitude within a few Kelvins, and the temperature at which that drop occurred could be tuned by changing the incident light intensity. Modeling the system with rate equations for competing electron-hole recombination flows through three defect species, one of which is a nonradiative deep donor, gives results consistent with these observations.

DOI: 10.1103/PhysRevB.84.075212 PACS number(s): 78.55.Cr, 71.55.Eq

I. INTRODUCTION

Gallium nitride (GaN) has attracted great interest over the past two decades as a material for blue and ultraviolet light emitting devices. There has been significant progress in both the preparation of high quality samples and the characterization of the properties of this semiconductor. However, point defects in GaN are not well understood. Photoluminescence (PL) provides one way of studying them, but only a few defect-related PL bands are identified with certainty.

Among these bands is the Zn-related blue luminescence (BL) band that exhibits the sharp drop in PL intensity reported here. This band has a maximum at 2.9 eV, a zero-phonon line at 3.1 eV, and a characteristic fine structure.[1–7] It is often observed in undoped *n*-type GaN that is grown either by metal-organic chemical vapor deposition (MOCVD) or hydride vapor phase epitaxy (HVPE) methods. In such samples, the BL band arises from uncontrolled contamination of GaN with Zn during growth.[8] It is also observed in Zn-doped GaN as the dominant PL band, where it is usually structureless. In both undoped and Zn-doped GaN this band is attributed to transitions from a shallow donor (at low temperature) or from the conduction band (at elevated temperatures) to the Zn_{Ga} acceptor.[8]

The energy level of the Zn_{Ga} acceptor above the valence band edge has been estimated to be 0.40 eV at 15 K and ~0.34 eV from 200 to 300 K (Ref. 8). Thus one would expect a *p*-type conductivity in GaN:Zn. However, all attempts to achieve such a *p*-type semiconductor have failed, and instead, semi-insulating samples with an unknown type of conductivity were produced in the past.[9–12] A reasonable but unconfirmed explanation of this failure is self-compensation of Zn_{Ga} acceptors by unknown deep donors during growth of GaN.

In previous works that reported less dramatic decreases of PL in GaN with increasing temperature, the thermal quenching of the BL band has been described in terms of an activation energy, and that approach has been controversial for many years. In undoped or Zn-doped *n*-type GaN, the Arrhenius plot reveals an activation energy of 300–400 meV (Refs. 2 and 13), which is consistent with the ionization energy of Zn_{Ga}. In sharp contrast, in some GaN:Zn samples an "activation energy" of 640 meV has been reported,[14] which is already unreasonably high. In the data reported here, for high-resistivity GaN samples doped with Zn, if one interprets the slope of the quenching of the BL band as an activation energy, that value would be about 1 eV, which makes no sense physically. In addition, the temperature of the quenching shifts significantly to higher temperatures with increasing excitation intensity. This behavior has never been reported for any defect-related PL in GaN. The unusual quenching of the BL band in Zn-doped GaN is consistent with a rate-equation model using acceptors, shallow donors, and deep nonradiative donors.

II. EXPERIMENT

A. Sample characterization

We studied nine Zn-doped GaN layers grown by the HVPE method on the *c*-plane sapphire (Table I). Seven of these (with prefixes of s and ap) were grown by TDI, Inc. in the period from 2001 to 2007, and two samples (1393 and 1394) were grown at the MIT Lincoln Lab in 2001. The thicknesses of the GaN layers given in Table I were estimated based on growth conditions and were verified in some cases by measurements of Fabry-Perot interference oscillations. The concentration [Zn] of Zn atoms in Table I has been determined by secondary ion mass-spectrometry (SIMS). The only sample that did not show the dramatic thermal quenching of PL reported in this paper was the one with the lowest concentration of Zn (ap275).

Some of the Zn-doped GaN samples from both TDI and MIT have been shown to have a high-resistivity

TABLE I. Characteristics of the GaN samples.

Sample	Source	Growth method	Doping	Thickness (μm)	[Zn] (cm^{-3})	Quantum efficiency for PL bands (%)			
						YL[a]	BL[a]	UVL[a]	Exciton[b]
s451	TDI	HVPE	Zn	2.9	5×10^{18}		30	0.4	0.02
s452	TDI	HVPE	Zn	2.9	2×10^{19}		25	0.1	0.004
s454	TDI	HVPE	Zn	2.9	6×10^{19}		1	10^{-4}	3×10^{-4}
s560	TDI	HVPE	Zn	5.0	unknown		25	1.5	0.03
ap269	TDI	HVPE	Zn	6.6	2.5×10^{18}		30	0.01	0.006
ap274	TDI	HVPE	Zn	4.8	1.7×10^{17}		25	0.07	0.03
ap275	TDI	HVPE	Zn	4.5	2.3×10^{16}		20	0.3	0.03
1393	MIT	HVPE	Zn	$\sim$10	$\sim 10^{18}$		20	<0.005	0.003
1394	MIT	HVPE	Zn	17.6	$\sim 10^{18}$		20	<0.005	0.003
th1011	TDI	HVPE	undoped	6.0	$<5 \times 10^{15}$		20	2	0.1
svt750	VCU[c]	MBE	undoped	3.0	unknown	1.0		0.05	0.01
r6623	VCU[c]	MBE	Si	7.6	unknown	0.1		80	0.15

[a]At 15–100 K and 10^{-4}–10^{-2} W/cm^2.
[b]At 100 K and 0.3 W/cm^2.
[c]Samples grown in the group of H. Morkoç.

(10^9–10^{12} ohm-cm) (Refs. 11 and 14). Exact resistivity values and whether the samples were p type or n type could not be unambiguously established since such measurements are difficult because of low hole mobility, poor Ohmic contacts in high-resistivity GaN, and possible potential fluctuations typical of compensated semiconductors.[15] Moreover, in GaN grown by the HVPE method, a highly conductive n-type layer is sometimes formed near GaN/sapphire interface due to contamination with oxygen.[16] This layer shunts the high-resistivity bulk region in the electrical measurements. However, in sample s560 we were able to establish weak p-type conductivity at room temperature with the hot probe method.

We also characterized several undoped n-type GaN samples grown by TDI under similar conditions. To compare the behavior of the BL band in Zn-doped and undoped samples, we have chosen a typical sample (th1011), for which the concentrations of free electrons, acceptors, and shallow donors were estimated from an analysis of the temperature-dependent Hall effect.[17] The free electron concentration was $n = 1.5 \times 10^{17}$ cm^{-3} at $T = 300$ K and $n = 5 \times 10^{16}$ cm^{-3} at $T = 200$ K. The concentrations of the shallow donors and of all types of acceptors were $N_D = 6.1 \times 10^{17}$ cm^{-3} and $\sum_i N_{\mathrm{A}i} = 3.1 \times 10^{17}$ cm^{-3}, respectively. The shallow donors in undoped GaN are usually $\mathrm{O_N}$ and $\mathrm{Si_{Ga}}$ centers.[8] Zn was not detected by SIMS in undoped GaN, which means that its concentration must be less than $\sim 5 \times 10^{15}$ cm^{-3}.

B. Photoluminescence measurements

Steady-state PL was excited with a continuous-wave He-Cd laser (50 mW, photon energy 3.81 eV). The PL signal was dispersed by a 1200 rules/mm grating in a 0.3 m monochromator and detected by a cooled photomultiplier tube. By using neutral density filters and an unfocussed laser beam with a diameter of 4 mm, the excitation power density (P_{exc}) was varied from 2×10^{-7} to 0.3 W/cm^2, while a focused beam with a diameter of 0.1–0.2 mm was used to obtain P_{exc} up to 200 W/cm^2. A closed-cycle optical cryostat and a high-temperature cryostat were employed for the temperature ranges of 13–330 K and 295–650 K, respectively. The PL spectra were corrected for the response of the optical system by comparing the spectrum of a tungsten lamp with a standard spectrum.

The absolute internal quantum efficiency η of PL is defined as $\eta = I^{\mathrm{PL}}/G$, where I^{PL} is the PL intensity (the number of photons emitted per second from unit volume) integrated over a specific spectral region and G is the concentration of electron-hole pairs created by above-band-gap illumination per second in the same volume. G was estimated from the excitation power density by taking the PL active layer to be $\alpha^{-1} \approx 0.1$ μm thick, where $\alpha \approx 10^5$ cm^{-1} is the absorption coefficient for GaN at 325 nm (Ref. 18).

To find η, we first estimated, using the method described in Appendix A, the absolute internal quantum efficiency from PL bands in the Si-doped GaN sample (r6623). This sample was later used as a standard to estimate the absolute internal quantum efficiency of the BL band and other PL bands (Table I) in GaN samples studied in this work by comparing integrated intensities of the PL bands with those obtained from the calibrated standard. All the samples were measured under identical conditions, and we assumed that the light extraction efficiency is the same for the samples and the standard. We estimate that possible errors in the absolute internal quantum efficiency of PL determined by this method do not exceed 30%. The shape and position of the BL band and other defect-related bands in GaN as a function of temperature are known from previous studies.[8] We used this information to deconvolute PL spectra where several PL bands overlapped. The errors due to this procedure are insignificant when compared with the changes in PL intensity observed in this work.

Additional information on defects in GaN is obtained from time-resolved PL measurements. We have estimated that the lifetime for the BL band is $\tau \approx 3$ μs and $\tau \approx 40$ μs at 180 K in HVPE-grown Zn-doped and undoped GaN, respectively. We have similarly estimated the lifetime for the yellow luminescence (YL) band to be $\tau \approx 600$ μs at 400 K in undoped GaN (sample svt750) grown by molecular-beam

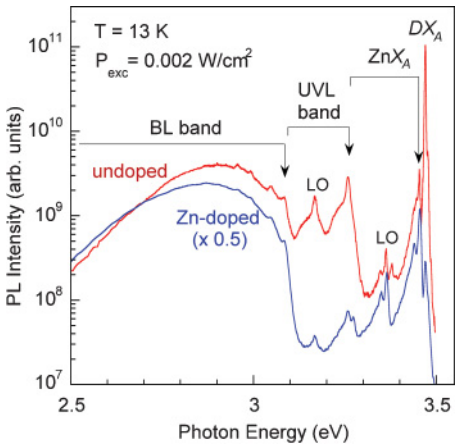

FIG. 1. (Color online) PL spectra from undoped GaN (sample th1011) and Zn-doped GaN (ap274), where $T = 13$ K and $P_{\text{exc}} = 0.002$ W/cm^2. Arrows indicate the zero-phonon lines for the BL and UVL bands and for the ZnX_A exciton. The Zn-doped data have been multiplied by 0.5.

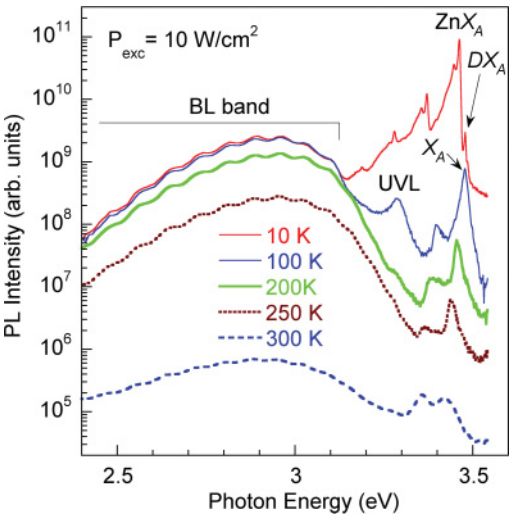

FIG. 2. (Color online) PL spectra from Zn-doped GaN (sample s451) at $P_{\text{exc}} = 10$ W/cm^2, for several temperatures. At 13 K, the ZnX_A exciton band consists of the zero-phonon line at 3.46 eV and three LO phonon replicas, at multiples of 92 meV at lover energies. At energies above ZnX_A, the DX_A and X_A zero-phonon lines can be seen as a peak and a shoulder, respectively. At 100 K and above, the exciton band consists of only the X_A line and its first LO phonon replica.

epitaxy (MBE). The electron- and hole-capture coefficients, C_{nA} and C_{pA}, for acceptors responsible for the BL and YL bands are known from previous studies.[8]

III. RESULTS

A. PL spectra in undoped and Zn-doped GaN

Although the abrupt quenching reported in this paper is observed only in Zn-doped samples, it is useful to compare PL data for Zn-doped samples with that for undoped samples to appreciate how dramatic the new effect really is. Figure 1 shows typical PL spectra at low temperature for undoped and Zn-doped GaN. In undoped GaN layers (the red curve), the excitonic luminescence (from 3.3 to 3.5 eV) includes a sharp and intense line at 3.47 eV attributed to the A exciton bound to a neutral shallow donor (DX_A) and a weaker peak at 3.455 eV attributed the exciton bound to the neutral Zn_{Ga} acceptor (ZnX_A). These peaks are followed by LO phonon replicas. The defect-related PL spectrum includes the ultraviolet luminescence (UVL) band (from 3.1 to 3.3 eV) with the main peak at 3.26 eV and an LO phonon replica, the BL band (from 2.2 to 3.1 eV) peaking at 2.9 eV, and a structureless red luminescence band (from 1.5 to 2.2 eV) with a maximum at 1.8 eV (not shown). The BL band reveals a characteristic fine structure. This includes a zero-phonon line at 3.085 eV and other peaks attributed to electron-phonon coupling involving two phonon modes, which are an LO mode with phonon energy of 91 meV and a local or pseudolocal mode with phonon energy of 36 meV (Ref. 6). This BL band is often observed in undoped n-type GaN grown either by the MOCVD or the HVPE method where it appears due to uncontrolled contamination of GaN with Zn during growth.[8] In MBE-grown undoped GaN, there is no BL band, and the YL band, with a maximum at 2.2 eV, is the dominant defect-related band.[8]

The PL spectrum from Zn-doped GaN (the blue curve in Fig. 1) is similar to that of undoped samples, but with the donor-bound exciton line and the UVL band greatly reduced. The fine structure in the BL band could only be resolved in the samples with a low concentration of Zn. Because the same characteristic fine structure is observed in both Zn-doped and undoped GaN, the BL band is attributed to the same transitions involving the Zn_{Ga} acceptor for both. These transitions are from a shallow donor (at low temperature) or from the conduction band (at elevated temperatures) to the Zn_{Ga} acceptor.[8]

For the Zn-doped GaN samples considered in this paper, the interesting range of temperatures is above 100 K and range of excitation intensities is below 10 W/cm^2. As can be seen in Fig. 2, at $P_{\text{exc}} = 10$ W/cm^2 and $T > 100$ K, the BL band is the dominant PL band. That is, the integrated intensity for the BL band is much larger than the integrated intensities of all the other bands combined. It becomes even more dominant as the excitation intensity decreases or the temperature increases. The exciton emission decreases superlinearly with decreasing excitation intensity. Note that the ZnX_A and DX_A bands quench at relatively low temperature, so that only the free exciton (X_A) and the UVL band contribute to the emission spectrum above 3.2 eV for temperatures above 100 K. These have relatively small quantum efficiencies (Table I) and quench rapidly above 100 K.

B. Thermal quenching in undoped GaN

To appreciate the dramatic results of the tunable abrupt quenching we have found in Zn-doped GaN, it is useful to review the typical features of thermal quenching that are commonly observed in conductive n-type GaN. For this purpose, we will analyze the BL band in HVPE-grown GaN (sample th1011) and the YL band in MBE-grown GaN (svt750). In conductive GaN the concentration of free electrons is nearly constant in the temperature range of quenching and much

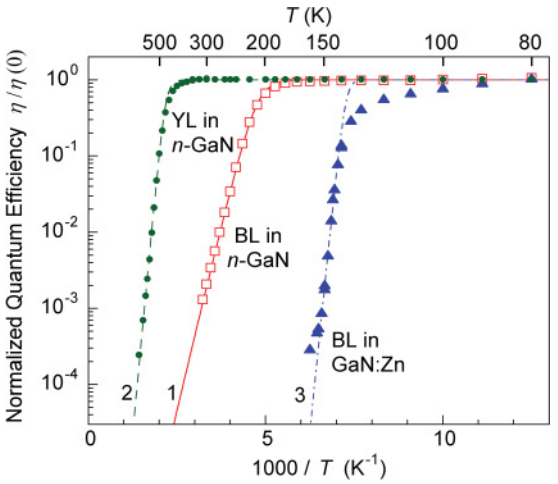

FIG. 3. (Color online) Temperature dependence of the BL band quantum efficiency in conductive undoped GaN (th1011, red squares) and high-resistivity Zn-doped GaN (s452, blue triangles). The temperature dependence of the YL band quantum efficiency in another undoped GaN sample (svt750) is shown for comparison (green circles). $P_{\rm exc} = 3 \times 10^{-5}$ W/cm^2. Lines are calculated using Eq. (1) with the following parameters: $\eta(0) = 0.15$, $E_A = 0.34$ eV, $\tau = 4 \times 10^{-5}$ s, and $C_{pA} = 10^{-6}$ cm^3/s ($\nu = 3.8 \times 10^{12}$ s^{-1} at 200 K)(curve 1); $\eta(0) = 0.01$, $E_A = 0.90$ eV, $\tau = 6 \times 10^{-4}$ s, and $C_{pA} = 10^{-6}$ cm^3/s ($\nu = 4.4 \times 10^{12}$ s^{-1} at 200 K)(curve 2); and $\eta(0) = 0.15$, $E_A = 0.90$ eV, $\tau = 3 \times 10^{-6}$ s, and $\nu = 10^{38}$ s^{-1} (curve 3).

larger than the concentration of photogenerated electrons. For this reason, the concentration of holes in the acceptor determines the temperature dependence of the quenching.

The quenching of the BL band in undoped GaN is shown in Fig. 3 as red open squares, and the linear slope on the semilog plot of quantum efficiency versus inverse temperature suggests that there is an activation energy $E_A \approx 0.35$ eV. In other words, the quantum efficiency is proportional to $\exp(E_A/kT)$, where k is Boltzmann's constant. Increasing the temperature reduces the hole concentration in the acceptor level, and this decreases the PL intensity. Similarly, the quenching of the YL band, which is shown in Fig. 3 as green filled circles, has an activation energy of $E_A = 0.9$ eV. This quenching, which begins at $T \approx 200$ K for the BL band and $T \approx 450$ K for the YL band, can be explained by thermal emission of holes from Zn_{Ga} and V_{Ga}-related acceptors, respectively, to the valence band and their consequent recombination via other radiative and nonradiative centers.[6,8,13] Therefore, for both these cases a simple model with a single activation energy for emission of holes explains the data, with the quantum efficiency $\eta(T)$ for a particular band given by[13]

$$\eta(T) = \frac{\eta(0)}{1 + \nu\tau \exp(-E_A/kT)}, \tag{1}$$

with

$$\nu = \tfrac{1}{2}[1 - \eta(0)] C_{pA} N_v, \tag{2}$$

and

$$C_{pA} = \sigma_{pA} \langle v \rangle, \tag{3}$$

where $\eta(0)$ is the low-temperature quantum efficiency, τ is the PL lifetime, ν is the characteristic frequency associated with the acceptor, E_A is the ionization energy of the acceptor, C_{pA} and σ_{pA} are the hole-capture coefficient and cross section for the acceptor, respectively, $\langle v \rangle$ is the mean velocity of free holes ($\sim 10^7$ cm/s in GaN at 200 K), and N_v is the effective density of states in the valence band ($\sim 10^{19}$ cm^{-3} in GaN at 200 K).

Fits of Eq. (1) to the quantum efficiency data for the BL and YL bands in n-type GaN are shown in Fig. 3 by the solid red and long-dashed green curves, respectively, with parameters given in the figure caption. In agreement with experiment, Eq. (1) predicts that the PL intensity is independent of temperature for $T < T_0$ and is proportional to $\exp(E_A/kT)$ for $T > T_0$, where T_0 is

$$T_0 = \frac{E_A}{k \ln(\nu\tau)}. \tag{4}$$

In the Arrhenius plot, T_0 is the temperature where two lines, corresponding to the temperature-independent and exponential parts, cross when extrapolated.

According to Eq. (4), there is nearly a linear dependence between T_0 and E_A (i.e., PL via deeper defects should start quenching at higher temperatures and will have a steeper slope). A good example is the YL band, which is attributed to an acceptor with ionization energy of $E_A = 0.9$ eV (Ref. 8). Parameters ν and τ are not much different for various acceptors in n-type GaN, and typical values of the hole-capture coefficient C_{pA} fall in the range of 10^{-7}–10^{-6} cm^3/s (Ref. 8). Thus, we expect that for larger E_A, PL quenching will begin at a *higher* temperature and with a larger slope in the semilog plot.

C. Thermal quenching of the BL band in Zn-doped GaN

The BL band in high-resistivity Zn-doped GaN samples exhibits strikingly different behavior from that in undoped samples. For low excitation intensity, the quenching of the BL band is extremely steep (with a slope ≈ 0.9 eV), and the quenching starts at temperatures much lower than for the undoped samples (see blue filled triangles in Fig. 3). The PL intensity decreases by two orders of magnitude over an interval that is only 10 K wide. Figure 4 shows the evolution of the PL spectrum in this temperature region. The shape and position of the BL band do not change in the process of the abrupt quenching. The abrupt quenching of the BL band was observed in eight Zn-doped GaN samples, as shown in Fig. 5 at a higher excitation intensity. As can be seen in this figure, the abrupt quenching is, in some samples, followed by much slower decrease of PL at temperatures above 250 K.

An important feature to note is that the sudden drop in PL shifts to higher temperatures with increasing generation rate (i.e., the quenching is tunable). This effect is demonstrated in Fig. 6, where we show several curves of quantum efficiency, one for each excitation intensity. In the initial analysis of the data we extrapolated the low-temperature part (which is almost horizontal) and the part with the largest slope to the point where they cross and defined the temperature of this crossing as the characteristic temperature T_0 at which the sudden quenching begins. This temperature is plotted in Fig. 7 as a function of the generation rate G for high-resistivity GaN:Zn samples. The slope of the dependence of $1/T_0$ on $\ln G$ is about the same for

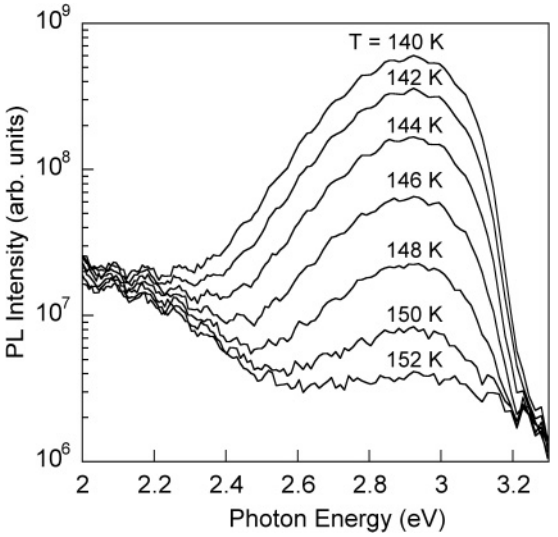

FIG. 4. Evolution of PL spectrum in high-resistivity Zn-doped GaN (sample s452) with increasing temperature from 140 to 152 K. $P_{\rm exc} = 3 \times 10^{-5}$ W/cm^2. The weak oscillations with the period of about 0.08 eV are due to the interference effect in the 3-μm-thick GaN layer.

all the samples. The abrupt and tunable thermal quenching of the BL band has been observed in all Zn-doped GaN samples except for the sample ap275, which has very low concentration of Zn (Table I) and is apparently conductive n type. This behavior is very different from typical quenching of PL in conductive n-type samples as discussed in Sec. III B.

Although Eq. (1) can be forced to fit the high-resistivity GaN:Zn data, as shown by the blue dot-dashed curve in Fig. 3, this is only done at the cost of a ridiculously large value of the parameter $\nu \sim 10^{38}$ s^{-1}. The hole capture cross section would then be $\sigma_{pA} \sim 10^{12}$ cm^2, which is several square kilometers.

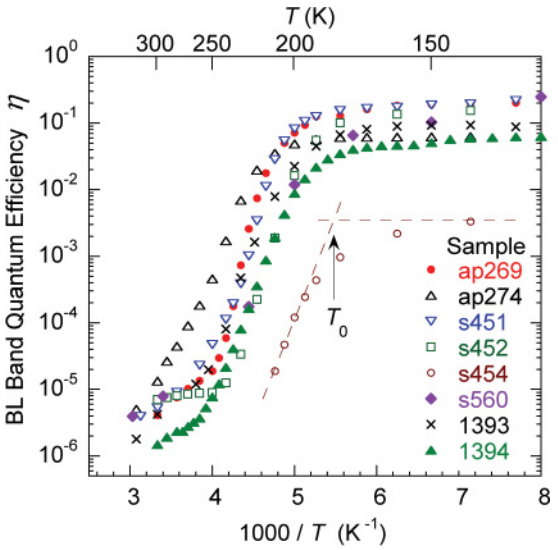

FIG. 5. (Color online) Temperature dependence of the quantum efficiency of the BL band for high-resistivity Zn-doped GaN samples. $P_{\rm exc} = 0.3$ W/cm^2. As an example, for sample s454, dashed lines are shown that cross at temperature defined as T_0.

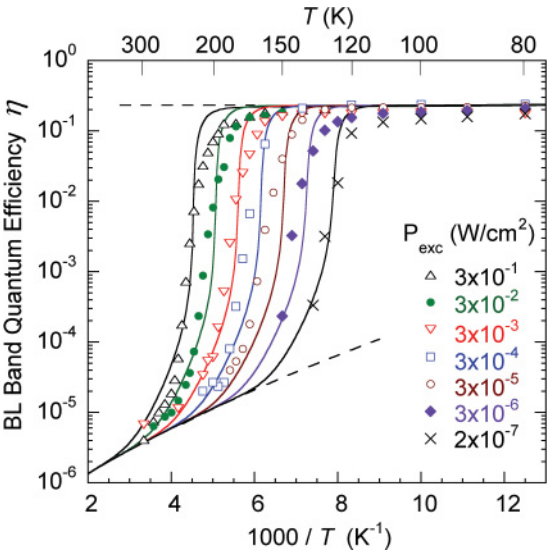

FIG. 6. (Color online) Temperature dependence of the quantum efficiency of the BL band in high-resistivity Zn-doped GaN (ap269) for excitation power densities $P_{\rm exc}$ between 2×10^{-7} and 0.3 W/cm^2. The solid curves are from the numerical solution of Eqs. (7)–(12) with the following parameters: $N_A = 3 \times 10^{17}$, $N_S = 1.5 \times 10^{17}$, $N_D = 1.3 \times 10^{17}$, $N_c = 5 \times 10^{14} T^{3/2}$, $N_v = 3.2 \times 10^{15} T^{3/2}$ (all in cm^{-3}); $C_{nS} = 10^{-7}$, $C_{nD} = 10^{-8}$, $C_{pS} = 3 \times 10^{-6}$, $C_{pA} = 10^{-6}$, $C_{nA} = 4 \times 10^{-13}$, $C_{DA} = 8 \times 10^{-12}$ (all in cm^3/s); $E_D = 30$ meV, $E_A = 350$ meV, and $g = 2$. $G = 1.6 \times 10^{23} \times P_{\rm exc}$ cm^{-3}s^{-1}. The upper dashed line is calculated with Eq. (B29) and the lower dashed line with Eq. (24) and $N_S^+ = N_S$. All other parameters are the same as for numerical solution.

Even if one tries to invoke another model of the form of Eq. (1), the parameters are equally absurd. For example, PL quenching for defects in semiconductors is often explained by the so-called configuration-coordinate model, in which the defect converts from radiative to nonradiative above a certain

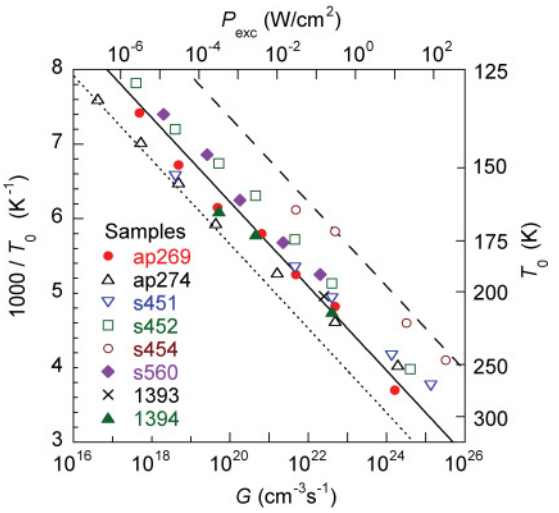

FIG. 7. (Color online) Dependence of the characteristic temperature T_0 on excitation intensity for high-resistivity Zn-doped GaN samples. The lines are calculated using Eq. (22) with $E_A = 350$ meV and different values of parameter B: 10^{30} (dotted line), 10^{31} (solid line), and 10^{33} cm^{-3}s^{-1} (dashed line).

temperature.[19,20] In this model, ν is the phonon frequency of the excited defect state and E_A is the energy barrier between the minimum of the excited state of the defect and the point where the adiabatic potentials of the excited and ground states cross.[21,22] Since a typical phonon frequency is $\nu \sim 10^{13}$ s^{-1}, the fitted value of 10^{38} is equally absurd for this model. Thus a new model is needed to explain the PL quenching in high-resistivity Zn-doped GaN.

D. Thermal quenching of the exciton band in Zn-doped GaN

Additional evidence for the necessity of a new model comes from the behavior of the quenching of the free exciton band. Typically, the quenching of defect-related bands causes a rise in the intensity of the exciton band, as explained in Appendix A. For example, in conductive n-type GaN the exciton emission intensity slightly *increases* simultaneously with the quenching of the BL band.[13]

However, in high-resistivity Zn-doped GaN, the free exciton band intensity decreases abruptly by orders of magnitude in the same temperature region as the BL band, as can be seen in Fig. 8, where the data for the BL band and the exciton band are shown by blue-filled circles and red triangles, respectively. The quantum efficiency of the exciton band decreases by orders of magnitude at about 220 K at $P_{\text{exc}} = 10$ W/cm^2. Unlike the BL band, the exciton band has an additional quenching behavior at lower temperatures with an apparent activation energy of about 25 meV. These features were observed in several high-resistivity Zn-doped GaN samples in which the exciton emission was strong enough to be analyzed reliably.

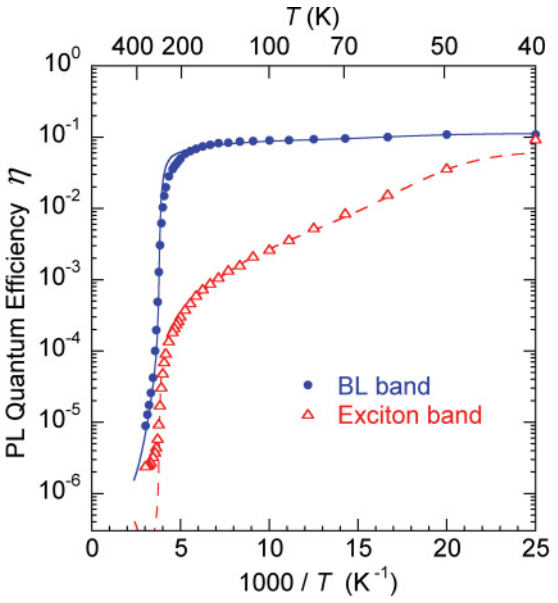

FIG. 8. (Color online) Temperature dependence of the quantum efficiency of the BL band (filled circles) and exciton band (empty triangles) for sample s451 with $P_{\text{exc}} = 10$ W/cm^2. The solid blue curve is calculated using Eqs. (7)–(12) with $N_A = 4.6 \times 10^{17}$, $N_S = 2.7 \times 10^{17}$, $N_D = 1.6 \times 10^{17}$ (all in cm^{-3}); $C_{pS} = 2.5 \times 10^{-6}$, $C_{DA} = 4 \times 10^{-12}$ (all in cm^3/s); and $G = 1.6 \times 10^{24}$ cm^{-3}s^{-1}. Other parameters are the same as for Fig. 6. The dashed red curve is calculated for the exciton emission quenching by using Eq. (29) with $E_x = 33$ meV, $\tau_x = \mathcal{K}T^{3/2}$ with $\mathcal{K} = 1.3 \times 10^{-12}$ s K$^{-3/2}$, $N_{cv} = 3.4 \times 10^{14} T^{3/2}$ cm^{-3}, $C_x = 10^{-4}$ cm^3/s, and with n and p calculated with the same parameters as for the solid blue curve.

IV. RATE EQUATION MODEL

To explain the dramatic behavior of PL in Zn-doped GaN, we propose a phenomenological rate-equation model for a semiconductor that could either be p type or n type. From characterization of the samples, as discussed in Sec. II A, the minimal set of centers participating in carrier recombination in both the HPVE-grown undoped and the Zn-doped GaN samples must include three types of point defects: the Zn_{Ga} acceptor, the O_{N} shallow donor, and an unknown nonradiative center. The Zn_{Ga} acceptor has an ionization energy of about 0.35 eV at temperatures between 100 and 300 K and is the dominant acceptor participating in PL process in these samples. Its electron- and hole-capture coefficients C_{nA} and C_{pA}, are known from previous studies (4×10^{-13} and 1×10^{-6} cm^3/s, respectively),[8] and its upper limit of concentration is roughly known from SIMS measurements (Table I). The O_{N} shallow donor, having the ionization energy of about 30 meV, is the dominant shallow donor causing n-type conductivity in undoped GaN.[8] Its concentration is typically in the 10^{17} cm^{-3} range. It is expected that incorporation of oxygen due to contamination during growth only increases when the sample is doped with an acceptor impurity such as Zn. Thus, the expected range of the O_{N} centers is 10^{17}–10^{18} cm^{-3}. A nonradiative center should be included to explain less than 100% quantum efficiency of radiative recombination (from all PL bands). While the identity of the nonradiative center is unknown, for certainty we will assume that it is a simple deep donor with unknown but reasonable capture parameters and concentration.

As illustrated by the band diagram shown in Fig. 9, our model describes a semiconductor with a direct band gap E_g, shallow donors D, acceptors A and nonradiative centers S, and these have total concentrations N_D, N_A, and N_S, respectively. The ionization energies for the shallow donors and acceptors are E_D and E_A. The thermal emission of electrons from the shallow donor D to the conduction band is indicated by an upward solid arrow, and the emission of holes from the

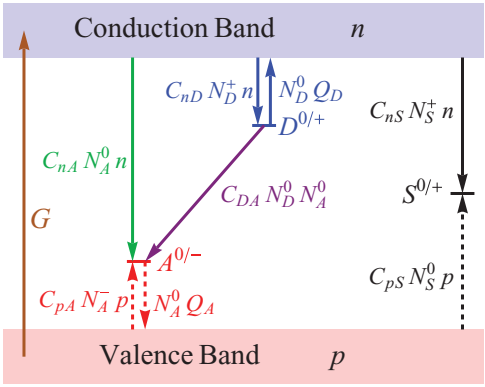

FIG. 9. (Color online) Band diagram and main transitions for a semiconductor with a shallow donor (D), acceptor (A), and a nonradiative deep donor (S). Transitions of electrons and holes are shown with solid and dashed arrows, respectively.

acceptor A to the valence band is indicated by a downward dashed arrow in Fig. 9. The rates of these transitions are described by the emission coefficients

$$Q_D = C_{nD} N_c g^{-1} \exp(-E_D/kT), \tag{5}$$

and

$$Q_A = C_{pA} N_v g^{-1} \exp(-E_A/kT), \tag{6}$$

where N_c and N_v are the effective densities of states in the conduction and valence bands, respectively, and g is the degeneracy factor of the donor and acceptor levels (assumed to be equal to 2 for both). These emission coefficients, which have units of s^{-1}, play an essential role in PL quenching. The nonradiative centers S have sufficiently deep donor level(s) that carriers cannot escape from them at temperatures used in our experiments. Otherwise we would see a simultaneous increase of the intensities of all PL bands, as discussed in Appendix A, but this was never observed. Therefore, our model does not include any thermal emission coefficients for these centers.

In high-resistivity GaN there are no free electrons and holes under dark conditions at low temperature. Illumination of a sample with a laser with energy greater than the band gap creates electron-hole pairs at a rate G per unit volume, as indicated by the large vertical upward arrow on the left-hand side of Fig. 9. These become the free electrons and holes with charge densities n and p, respectively. Although these charge carriers may form excitons, this process is only appreciable at low temperatures and high excitation intensities, as we discussed in Sec. III D. Because of their low concentrations, excitons play no role in the abrupt quenching of the BL band, and so are not included in the model. However, the free electrons may be captured nonradiatively by the shallow donors D and deep donors S, as indicated by the downward vertical solid arrows to D and S. Holes may be captured nonradiatively by A and S centers, as indicated by the upward dashed arrows. The only radiative transitions shown in Fig. 9 as downward green and purple solid arrows, are those from the shallow donor D and from the conduction band to the acceptor A, both of which combined give the BL band in GaN.

We use the traditional description of transition rates as the product of the concentrations of available carriers and available empty sites, multiplied by a constant factor called the capture coefficient.[22,23] In particular, C_{nD}, C_{nA}, and C_{nS} are the electron-capture coefficients for the donor, acceptor, and nonradiative defect, respectively; C_{pA} and C_{pS} are the hole-capture coefficients for the acceptor and nonradiative defect, respectively; and C_{DA} is the effective coefficient for donor-acceptor pair (DAP) recombination. N_D^+, N_D^0, N_S^+, N_S^0, N_A^0, and N_A^- are the concentrations of the D, S, and A centers in different charge states.

The rate equations under steady-state conditions can easily be written down from the band diagram in Fig. 9. Several terms contribute to the rate of change of free electron concentration n. Free electrons are generated by incident light at a rate G per unit volume and by thermal emission from the shallow donor at rate $Q_D N_D^0$. The conduction band loses electrons when they make transitions to the shallow donor D at rate $C_{nD} N_D^+ n$ and to the deep donor at rate $C_{nS} N_S^+ n$. Our first equation is thus

$$\frac{\partial n}{\partial t} = G - C_{nS} N_S^+ n - C_{nD} N_D^+ n - C_{nA} N_A^0 n + Q_D N_D^0 = 0. \tag{7}$$

The next equation describes the rate of change of the free hole concentration p. Holes are created at generation rate G and by thermal emission from the acceptor A at rate $Q_A N_A^0$. They are captured by the acceptor A at rate $C_{pA} N_A^- p$ and by the deep donor at rate $C_{pS} N_S^0 p$, so that

$$\frac{\partial p}{\partial t} = G - C_{pS} N_S^0 p - C_{pA} N_A^- p + Q_A N_A^0 = 0. \tag{8}$$

A third equation describes the gain and loss of electrons by the shallow donors D. Donors gain electrons by capture from the conduction band at rate $C_{nD} N_D^+ n$. They lose electrons by radiative transitions to the acceptor at rate $C_{DA} N_D^0 N_A^0$ and by thermal emission to the conduction band at rate $Q_D N_D^0$, so that

$$\frac{\partial N_D^0}{\partial t} = C_{nD} N_D^+ n - Q_D N_D^0 - C_{DA} N_D^0 N_A^0 = 0. \tag{9}$$

We also need the rate of change of electron concentration at the deep donor S, which can gain electrons by capturing them from the conduction band with rate $C_{nS} N_S^+ n$. It also loses electrons due to hole capture from the valence band at rate $C_{pS} N_S^0 p$, yielding,

$$\frac{\partial N_S^0}{\partial t} = C_{nS} N_S^+ n - C_{pS} N_S^0 p = 0. \tag{10}$$

The last rate equation describes the rate of change of electron concentration at the acceptor A. Electrons are gained by radiative transfer from the donor D at rate $C_{DA} N_D^0 N_A^0$ and from the conduction band at rate $C_{nA} N_A^0 n$ and by thermal excitation from the valence band at rate $Q_A N_A^0$. Electrons are lost by transfer to the valence band at at rate $C_{pA} N_A^- p$. Equivalently, these last two terms can be regarded as thermal emission of holes to the valence band and capture of holes from the valence band. The resulting rate equation is

$$\frac{\partial N_A^0}{\partial t} = C_{DA} N_D^0 N_A^0 + C_{nA} N_A^0 n - C_{pA} N_A^- p + Q_A N_A^0 = 0. \tag{11}$$

Finally, charge is conserved, and equating the sums of positive and negative charges gives

$$p + N_S^+ + N_D^+ = n + N_A^-. \tag{12}$$

The radiative DAP transition is actually a tunneling transition of an electron from a shallow donor D to an acceptor A. The probability of tunneling depends on the size of the electron wave function and the distance between D and A. Since there is a random distribution of these distances, this causes the transition rate to vary widely for pairs separated by different distances. We use here the average capture coefficient C_{DA} to describe all such DAP transitions. Although in conductive n-type GaN electron transitions from the conduction band to an acceptor (eA transitions) are much less probable than the DAP transitions below 50 K and become substantial above,[8] in high-resistivity Zn-doped GaN the DAP transitions are expected to dominate up to considerably higher temperatures.

This is because, first of all, the concentration of free electrons is very small, and second because the wave-function overlap between the shallow donor electrons and the acceptor holes is relatively large due to their high concentrations.

The DAP and eA transitions are often unresolved in the PL spectrum, especially in the case of broad PL bands, because the value of E_D is typically much smaller than the PL band width. Thus the quantum efficiency of the BL band is the sum of the two contributions and is given by

$$\eta = \eta_{\mathrm{DAP}} + \eta_{eA}, \tag{13}$$

where

$$\eta_{\mathrm{DAP}} = \frac{C_{DA} N_D^0 N_A^0}{G} \tag{14}$$

and

$$\eta_{eA} = \frac{C_{nA} N_A^0 n}{G}. \tag{15}$$

This equation assumes that G is a constant over the depth of penetration of light, given by the inverse absorption coefficient α^{-1}. The quantum efficiency can also be written in terms of the net flow of electrons from the acceptor to the valence band as

$$\eta = \frac{C_{pA} N_A^- p - Q_A N_A^0}{G}. \tag{16}$$

We solve numerically the set of nonlinear equations (7)–(12) and find good agreement with the experimental data shown in Fig. 6, where the solid curves are the numerical solution using the parameters given in the caption. As can be seen, the model explains both the abruptness of the quenching and the excitation dependence. As we mentioned in Sec. II many of these parameters are experimentally measured and others have quite restrictive ranges of reasonable magnitudes. All the nonradiative transitions have lifetimes of the order of 10^{-10} s, while the radiative transitions have lifetimes that are several orders of magnitude larger. For most of the defects in GaN, radiative lifetimes are of the order of 1 μs or more,[8] which provides a constraint on the relative values of all the capture coefficients. The parameters E_A, C_{nA}, and C_{pA} were determined from the quenching of the BL band and time-resolved PL in conductive n-type GaN samples, and the value of $E_D \approx 30$ meV is known from the exciton PL spectroscopy.[8] From the temperature-dependent Hall effect in undoped n-type GaN, we have determined the reasonable order of magnitude of concentrations of shallow donors and acceptors to be of the order of 10^{17} cm^{-3}. Therefore, the flexibility in choosing parameters to fit the data is very limited due to this large body of experimental information about these samples. It is clear that the model explains both the abruptness of the quenching and the excitation dependence, which was not possible with the simpler model described by Eq. (1) of Sec. III B.

The tunable abrupt quenching actually represents a crossover from one type of behavior of the system to another at a characteristic temperature T^*. Just below T^*, all of the deep donors S are neutral (i.e., filled with electrons) and the quantum efficiency of this nonradiative channel is about 80%, with the other 20% through the radiative DAP transition, and a negligible fraction through the eA transition. Above T^*, almost all deep donors are empty (i.e., depleted of electrons or filled with holes), and nearly 100% of carrier recombination occurs through the S center, resulting in a drop of orders of magnitude in the radiative DAP and eA transitions.

To gain insight into the reasons for this crossover in behavior, the abruptness of the crossover, and the temperature dependence of T^*, it is useful to analyze Eqs. (7)–(12) and obtain approximate analytic solutions for various temperature ranges, and especially for the temperature region around the crossover. We have given detailed derivations in Appendix B, and here we will summarize the main points. We first describe the case of a high-resistivity p-type semiconductor (Sec. IV A). For comparison, since there is not absolute certainty that all the samples were indeed p type, we will consider in Sec. IV B an n-type high-resistivity semiconductor. To show that this model encompasses the usual PL quenching, we will consider a conductive n-type semiconductor in Sec. IV C. In Sec. IV D, we will show that the temperature dependence of the exciton-band quenching is consistent with the model.

A. High-resistivity p-type semiconductor

Here we consider a high-resistivity p-type semiconductor with a shallow donor, a relatively deep acceptor, and a nonradiative donor. This specific model, in which $N_A > N_D + N_S$, yields the solid curves in Fig. 6. We begin the discussion with the region of temperature below T^*, which for $P_{\mathrm{exc}} = 0.3$ W/cm^2 is the approximate temperature range 100 K$< T <$ 200 K shown in Fig. 10. Figures 10 and 11 show the various concentrations along with the resulting quantum efficiencies calculated numerically. Figure 10 is plotted with concentrations and quantum efficiencies on a

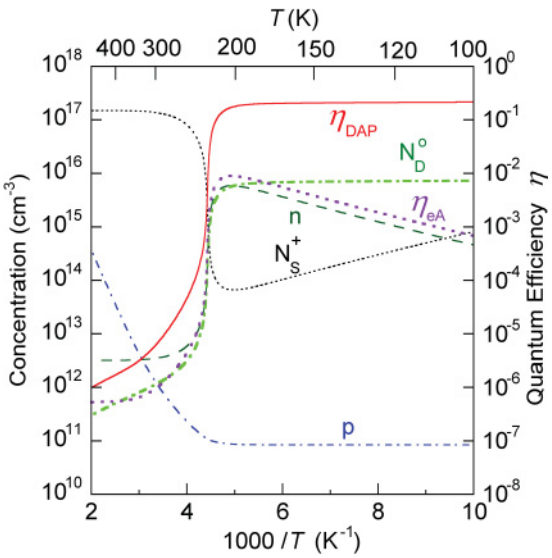

FIG. 10. (Color online) Calculations for a high-resistivity p-type semiconductor, showing temperature dependences of concentrations of free electrons (n), holes (p), neutral shallow donors (N_D^0) and positively charged S centers (N_S^+), and quantum efficiencies of the DAP and eA emission. The parameters are the same as were used in Fig. 6 with $P_{\mathrm{exc}} = 0.3$ W/cm^2 ($G = 4.8 \times 10^{22}$ cm^{-3}s^{-1}).

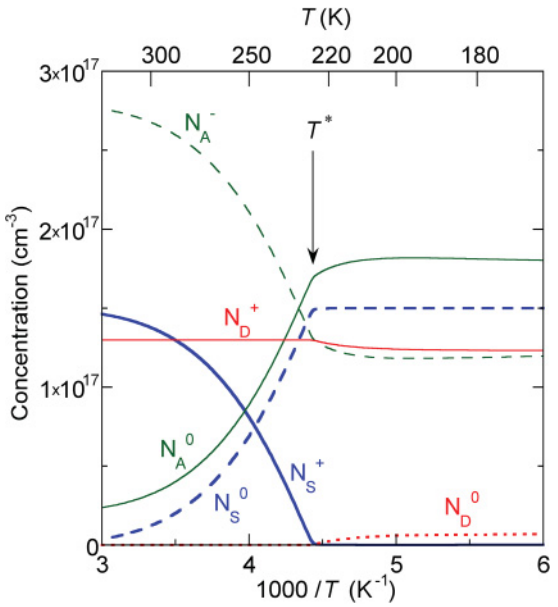

FIG. 11. (Color online) Calculations for a high-resistivity p-type semiconductor, showing temperature dependences of concentrations of charged and neutral defects. All parameters are the same as in Fig. 10.

logarithmic scale versus inverse temperature, and Fig. 11 is a linear plot of the larger concentrations over a smaller range of inverse temperatures. These plots illustrate the relative importance of each variable as the temperature approaches the crossover.

In the dark the S centers are completely empty, but for an excitation power $P_{\rm exc} < 1$ W/cm^2 they are 99.5% filled with electrons at 100 K, while the shallow donors are almost completely depleted of electrons ($N_D^+ \approx N_D$). The S centers become almost completely filled ($N_S^0 \approx N_S$) with increasing temperature, as exemplified by the decrease of N_S^+ with the activation energy of E_D, as shown by the dotted black curve in Fig. 10. This is because the free electrons, after being captured by shallow donors, may escape back to the conduction band before they recombine with holes via the DAP transition. This leads to a gradual increase of n with the same activation energy E_D. The increased concentration of electrons in the conduction band, combined with their fast capture by S centers, leads to the corresponding decrease in N_S^+. However, when the temperature increases sufficiently, holes can be emitted by the acceptor, and this breaks the bottleneck in the S channel.

Although the dramatic change in concentrations results from a complicated interaction between the acceptors, free holes, and S centers, one can see evidence for what happens by considering the changes in concentration of free holes. Up to a temperature very close to the crossover T^*, the only holes in the valence band are those that are optically generated, with a concentration

$$p \approx p_0 = \frac{G}{C_{pS}N_S + C_{pA}N_D}, \tag{17}$$

which is obtained from Eq. (B11) of Appendix B with N_S^+ and Q_A set to zero.

As the temperature approaches T^*, the thermal emission of holes from the acceptor level to the valence band cannot be ignored and the thermal contribution $p_{\rm th}$ can be included approximately by keeping the term containing $Q_A(N_A - N_S)$ in Eq. (B11) and substituting for Q_A from Eq. (6), with the result

$$\begin{aligned} p &= p_0 + p_{\rm th} \\ &= p_0\left[1 + \frac{C_{pA}(N_A - N_D)N_v}{gG}\exp\left(-\frac{E_A}{kT}\right)\right]. \end{aligned} \tag{18}$$

The hole concentration p increases with temperature and, as $T \to T^*$, it approaches a characteristic value

$$p \to p_{\rm lim} = \frac{G}{C_{pS}N_S}, \tag{19}$$

above which the concentration of electrons at the S centers must become much less than N_S. This is because, according to Eq. (8), the hole capture rate $C_{pS}N_S^- p$ must be less than G at any temperature. In such a situation, the entire recombination current would be through the S channel, assuming that the S level were filled with electrons.

Therefore, as the concentration of holes approaches $p_{\rm lim}$, the value of N_S^+ starts increasing dramatically because additional holes are available to open the bottleneck in the S channel. The concentration of ionized S centers (N_S^+) changes by orders of magnitude, from $N_S^+ \ll N_S$ to $N_S^+ \approx N_S$, in a narrow temperature range (close to $1000/T^* = 4.43$ K^{-1} in Figs. 10–12). In this same temperature range p changes by about 20%. This abrupt change in N_S^+ is accompanied by a drastic decrease in the concentration of free electrons because many more holes are now available at S centers for recombination. There is also an abrupt decrease in the concentration of electrons at donors. The drops in the concentrations of electrons in the conduction band and at donors result in drops in the DAP and eA quantum efficiencies because the availability of free electrons is crucial for these transitions, as is evident from Eq. (13).

In Appendix B, we show that Eqs. (7)–(12) can be reduced to a cubic equation in N_S^+, given by Eq. (B12), and that the other concentrations can be obtained from this. The quantum efficiency obtained from the solution of this cubic equation, Eq. (B18), is indistinguishable from the numerical solution, which is the black solid curve in Fig. 12. Below and up to a few degrees above the crossover temperature T^*, the cubic equation can be reduced to a quadratic solution for N_S^+, given by Eq. (B26), and the quantum efficiency obtained from that solution is shown by the blue dashed curve with squares. From less than 1 K above the crossover to above 300 K, the cubic equation reduces to a different quadratic, with the solution given by Eq. (B20), and the quantum efficiency obtained from that is shown as the red dotted curve. The flat black dotted line at the top is the linear extrapolation of the lower temperature solution, given by Eq. (B29) and the lower black dotted line is the linear extrapolation from higher temperatures, given by Eq. (B24) with $N_S^+ = N_S$.

With a slight change in notation, the approximate PL quantum efficiency in the temperature range from 100 K to very close to T^*, from Eq. (B28) in Appendix B, is

$$\eta = \eta_0[1 - \xi\exp(-E_A/kT)], \tag{20}$$

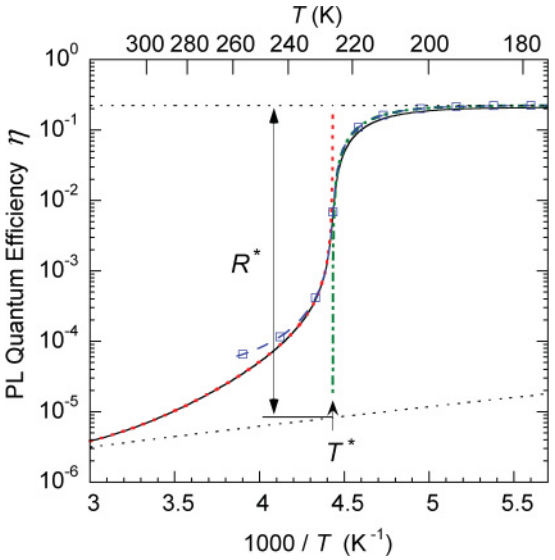

FIG. 12. (Color online) Temperature dependence of the quantum efficiency η of PL including DAP and eA components near T^*. The black solid curve is the numerical solution of Eqs. (7)–(12). The dashed blue curve with squares is approximate solution obtained using Eq. (B18) with N_S^+ from Eq. (B26). The dot-dashed green curve for $T < T^*$ is obtained with Eq. (20). The dotted red curve for $T > T^*$ is obtained with Eq. (24) with N_S^+ from Eq. (26). The top dotted black curve is obtained with Eq. (B29) and the bottom dotted black curve is obtained with Eq. (B24) with $N_S^+ = N_S$. All parameters are the same as in Figs. 10 and 11.

where

$$\xi = \frac{C_{pS} N_S (N_A - N_D) N_v}{g G N_D}. \tag{21}$$

and η_0 is given by Eq. (B29) in Appendix B. The green dot-dashed curve in Fig. 12 is calculated with Eq. (20).

The crossover temperature T^* at which the abrupt quenching of the acceptor-related PL takes place can be found by equating Eqs. (18) and (19) and rewriting in terms of η_0 from Eq. (B29), which gives

$$T^* = \frac{E_A}{k \ln(B/G)}, \tag{22}$$

with

$$B = C_{pA} \left(\frac{1}{\eta_0} - 1 \right) (N_A - N_D) \frac{N_v}{g}. \tag{23}$$

As explained in Appendix B, this is the same temperature at which the zeroth order approximation for N_S^+ at a temperature above T^* drops to zero and leads to Eqs. (B22) and (B23). Of course, substituting Eq. (22) into the expression for the quantum efficiency in Eq. (20) causes η to become zero, which is unphysical, but this equation is only the zeroth order approximation at this temperature. Since N_S^+ increases rapidly in the crossover region, it can no longer be ignored, and when a more accurate expression is used, as in Eq. (B18) of Appendix B, this problem never arises.

According to Eq. (22), the characteristic temperature T^* increases with excitation intensity, and the region of PL quenching shifts to higher temperatures (Fig. 6). The solid curve in Fig. 7 is obtained with Eq. (22) with $E_A = 350$ meV and $B = 10^{31}$ cm^3/s. The data for all high-resistivity samples can be fit fairly well with the same activation energy and parameter B within the range of 10^{30}–10^{33} cm^3/s.

After the abrupt drop, the quantum efficiency of the S channel becomes almost 100%. At temperatures above T^*,

$$\eta \approx \zeta \left(\frac{N_A - N_D - N_S^+}{N_S^+} \right) \tag{24}$$

with

$$\zeta = \frac{C_{DA}}{C_{nS}} \frac{g N_D}{N_c} e^{E_D/kT} + \frac{C_{nA}}{C_{nS}}, \tag{25}$$

and

$$N_S^+ = \tfrac{1}{2}(N_A - N_D + N_S + N_2) - \tfrac{1}{2}\sqrt{(N_A - N_D - N_S + N_2)^2 + 4N_2(N_D + N_S)}, \tag{26}$$

where $N_2 = (C_{pA} G)/(C_{pS} Q_A)$, and Q_A is defined with Eq. (6). These are the same as Eqs. (B24), (B8), and (B25), respectively, in Appendix B.

The value of the drop R^* in η at $T \approx T^*$ can be estimated as the ratio of the values given by the two linear extrapolations from low and high temperature, respectively, as shown in Fig. 12. This results in

$$R^* = \frac{\eta_0 N_S}{\zeta^* (N_A - N_S - N_D)}, \tag{27}$$

where ζ^* is the value of ζ in Eq. (25) evaluated at T^*. For the parameters of Fig. 12, $\zeta^* \approx 6 \times 10^{-5}$ and $R^* \approx 3 \times 10^4$. It is useful to write Eq. (27) in terms of η_0 instead of using its expression given by Eq. (B29) because this value can be determined experimentally. From Eq. (27) we can see that the value of the drop in quantum efficiency is large when ζ^* is small. This occurs when C_{DA} and C_{nA} are both small compared with C_{nS}, which is typical for optical transitions that are much slower than nonradiative capture. It is also favorable to have a sample with a high degree of compensation (i.e., when $N_S + N_D \to N_A$). The value of the drop also increases with increasing excitation intensity because then T^* increases.

The steepness of the slope can be estimated by considering the solution of the equations at T^*. The log slope of the quantum efficiency is

$$\frac{d(\ln \eta)}{d(1/T)} \approx \frac{E_A/k}{2\sqrt{\zeta^* \lambda}}, \tag{28}$$

where λ is given by Eq. (B35). For the parameters of Fig. 12, $\lambda \approx 15.4$, and $d(\ln \eta)/d(1/T) \approx 16 E_A/k$, which corresponds to an "activation energy" of 5.7 eV. In Fig. 13, the long-dashed line has this slope, and it agrees with the slope of the calculated curve, shown as the solid black curve, at the crossover temperature T^* We see that it is the small quantity ζ^* in the denominators of both R^* and of the logarithmic slope that leads to both the large drop and the steepness of the slope in the abrupt quenching.

The experimentally observed PL drop at $T = T^*$ is less abrupt than the calculated one, and it is sample dependent, as can be seen in Figs. 6 and 5. In different GaN:Zn samples, for different excitation intensities, the slope of the abrupt quenching versus temperature corresponds to an "activation

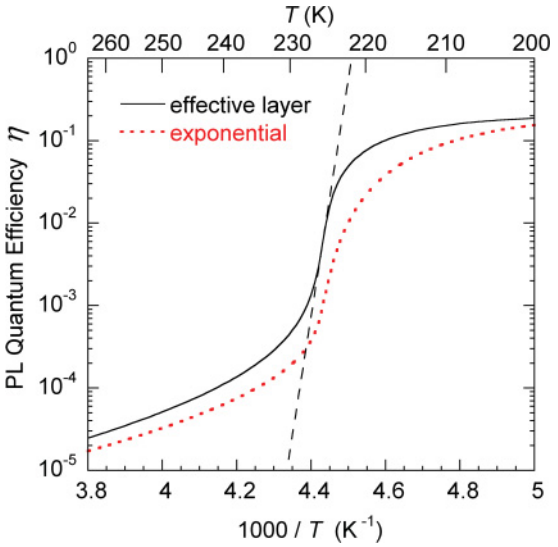

FIG. 13. (Color online) The acceptor-related PL quantum efficiency at temperatures close to the abrupt quenching for a high-resistivity p-type semiconductor. The solid black and dotted red curves are the numerical solution of Eqs. (7)–(12) with parameters as in Fig. 12, with the assumption that the excitation intensity is not changing in the effective depth equal to inverse absorption coefficient α^{-1} (solid black curve) and with the assumption that the excitation intensity decreases as $\alpha \exp(-\alpha x)$ where $\alpha = 10^5$ cm^{-1} and $x = 0$ at semiconductor surface (dotted red curve). The dashed line shows the dependence $I^{\mathrm{PL}} \propto \exp(E_{\mathrm{eff}}/kT)$ with $E_{\mathrm{eff}} = 5.7$ eV.

energy" varying between 600 and 1000 meV. This rounding or blurring of the drop might be due to a decrease in incident light intensity with depth. Indeed, for the calculations discussed earlier in this section, we have assumed that within an active layer of thickness α^{-1}, where α is the absorption coefficient, the generation rate G is constant. This corresponds to the calculated curves in Figs. 6 and 10–12 and to the solid black curve in Fig. 13. However, if we account for the exponential decrease of the excitation light intensity inside the semiconductor by integrating the PL intensity arising from different depths,[24] the position and shape of the abrupt transition change only slightly, as shown by the red dotted curve in Fig. 13 (the slope decreases by only 25% and the value of $1/T^*$ increases by less than 10^{-5} K^{-1}). Diffusion of photogenerated carriers was disregarded because the diffusion length of holes in high-resistivity GaN at low excitation intensity is expected to be less than 0.1 μm (Refs. 25 and 26).

There are other possible explanations for the blurring of the crossover. One is that there may be several types of nonradiative defects present in the samples, with one of them dominant in the competition between recombination channels. Another explanation is that there may be potential fluctuations in high-resistivity semiconductors that occur because of a random distribution of charged defects.[15,27] Both of these would be sample dependent and might explain why the largest slope of the drop in PL in the semilog plot versus temperature is sample dependent with the effective energy of the "activation" varying between 600 and 1000 meV in different GaN:Zn samples.

B. High-resistivity n-type semiconductor

An inspection of Fig. 6 shows that we were unable to confirm in all cases that the high-temperature slope approached the lower dashed line with slope E_D, particularly in cases of low incident power levels. For this reason, we now consider a high-resistivity n-type semiconductor in which $N_D + N_S > N_A > N_D$ and the Fermi level is close to the S level in the dark. For these conditions, acceptors are completely filled with electrons, shallow donors are empty, and the S centers are partially filled with electrons. Under illumination, as for the p type, the electron population of the S centers increases and the acceptors become partially filled with holes. The sharp drop in the curves occurs at about the same crossover temperature T^* (Fig. 14). However, at higher temperatures beyond this drop, the computed quantum efficiency decreases as $\exp[(E_A + E_D)/kT]$, that is, with an activation energy $E_A + E_D$ in place of E_D.

Compared with the p-type case, the concentrations of various carriers are similar below the crossover but quite different above the crossover, as can be seen from Figs. 15 and 16, as compared with Figs. 10 and 11. Above the crossover, $T > T^*$, N_A^0 decreases as $\exp(E_A/kT)$, and the concentration p of free holes is independent of temperature. Both the DAP and eA quantum efficiencies decrease with activation energy close to E_A, and the total PL signal decreases as $\eta \propto \exp(E_A + E_D)/kT$.

The PL quantum efficiency can still be approximated by Eqs. (20) and (24) for a temperature below and above T^*, respectively. The quenching of the PL in this case is reminiscent of the PL quenching in a conductive n-type semiconductor in that it shows an activation energy close to E_A (when $E_A \gg E_D$) and continues without any saturation. However, the overall behavior of the PL is quite different because the PL quantum efficiency above the crossover is much

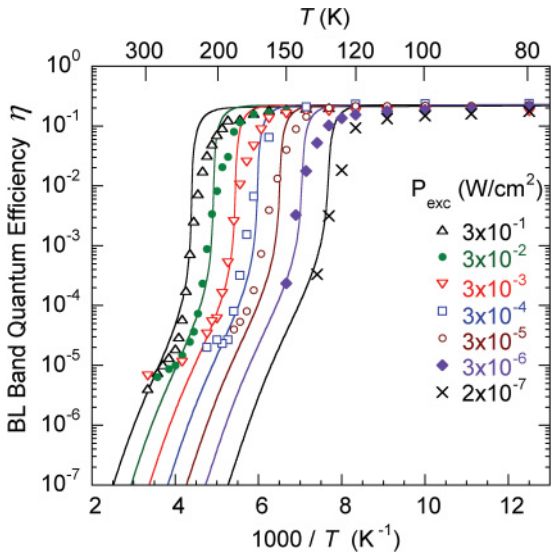

FIG. 14. (Color online) Temperature dependence of the quantum efficiency of the BL band in high-resistivity Zn-doped GaN (ap269), where the experimental points are the same as in Fig. 6. The solid curves are the numerical solution of Eqs. (7)–(12) for the case of a high-resistivity n-type semiconductor with $N_A = 2.7 \times 10^{17}$ cm^{-3}. Other parameters are the same as in Fig. 6.

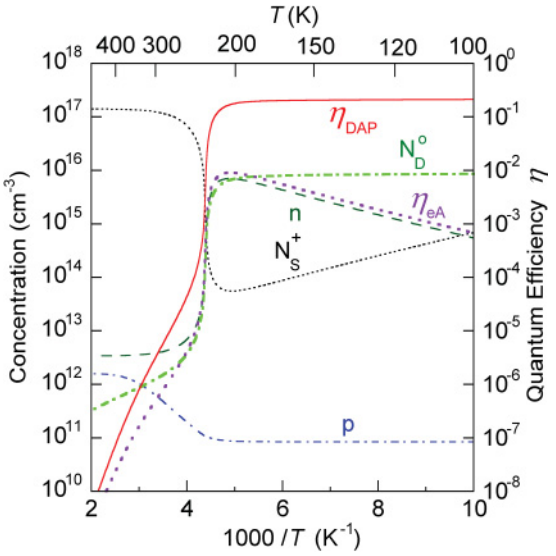

FIG. 15. (Color online) Calculations for a high-resistivity n-type semiconductor for the same quantities as in Fig. 10, for $N_D + N_S > N_A > N_D$, with $N_A = 2.7 \times 10^{17}$ cm^{-3}. Other parameters are the same as in Fig. 6 with $P_{exc} = 0.3$ W/cm^2 ($G = 4.8 \times 10^{22}$ cm^{-3}s^{-1}).

smaller than it would be for the conductive case and strongly depends on excitation intensity, in contrast to T_0 in Eq. (4).

The abrupt quenching of PL with the crossover temperature T^* tunable with excitation intensity is a signature of all high-resistivity semiconductors. In addition, one can determine whether the semiconductor is n or p type from the behavior of the PL quantum efficiency at temperatures above the abrupt drop. The experimental dependences shown in Fig. 5 indicate that at least some GaN:Zn samples are p type since the data do appear to approach a slope of E_D rather than E_A. This

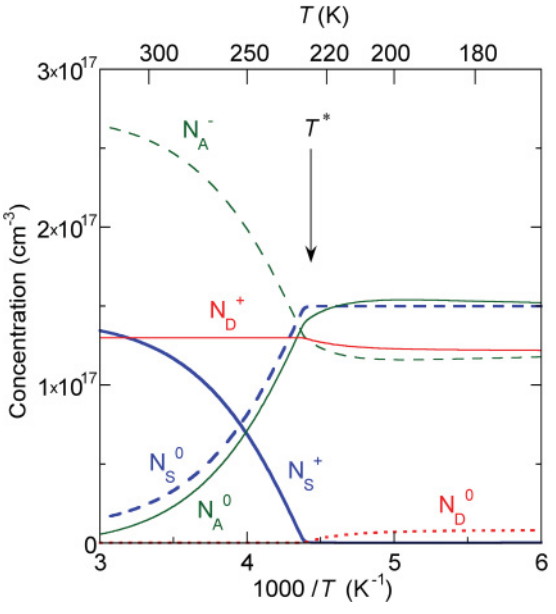

FIG. 16. (Color online) Calculations for a high-resistivity n-type semiconductor, showing temperature dependences of concentrations of the same charged and neutral defects as in Fig. 11. All parameters are the same as in Fig. 15.

could only be seen at the higher excitation powers for which the sensitivity of our PL set-up allowed for reliable detection beyond the crossover.

C. Conductive n-type semiconductor

In a conductive n-type semiconductor, $N_D > N_A$ and the Fermi level is close to the conduction band. Acceptors and nonradiative defects are completely filled with electrons, making $N_A^- = N_A$, while shallow donors are only partially filled with electrons in the dark. At sufficiently low excitation intensity, such that the PL intensity increases linearly with excitation intensity, the concentration of holes at the acceptors is negligible, and the PL quantum efficiency due to eA transitions is given by Eq. (1), where $\tau = 1/C_{nA}n$ (Refs. 8 and 13).

For conductive n-type semiconductors, in the case of low excitation intensity ($N_A^0 \ll N_A$ and $N_S^+ \ll N_S$), Eq. (1) can be derived from Eqs. (7)–(12). Quenching of the acceptor-related PL band begins when the second term in the denominator of Eq. (1) becomes comparable to unity [i.e., at T_0 defined by Eq. (4)]. The activation energy of this quenching is approximately equal to E_A (reduced slightly due to the temperature dependence of N_v).[13] Since T_0 is independent of G, the temperature dependence of the defect-related PL quantum efficiency is expected to be independent of excitation intensity, which has, in fact, been observed in our experiments on n-type GaN. Numeric calculations using Eqs. (7)–(12) give essentially the same result as in the simplified model presented in Ref. 13 because the differences in the models (the lack of DAP luminescence in Ref. 13) are hidden in the parameter τ, which can be determined experimentally.

D. Quenching of exciton emission in high-resistivity Zn-doped GaN

Our model also explains the sudden quenching of the exciton luminescence at $T \approx T^*$ (Figs. 2 and 8). At low temperatures ($T < 50$ K) the exciton emission is dominated by annihilation of the acceptor-bound excitons ZnX_A, and at higher temperatures the free exciton emission X_A dominates (Fig. 2). The binding energies of the ZnX_A exciton (24 meV) and the X_A exciton (26 meV) are close to each other,[8] so that when the intensity, integrated over the entire excitonic spectrum, is plotted versus the inverse temperature, a single slope corresponding to an activation energy of about 25 meV is observed in the temperature range of 40–150 K (Fig. 8). However, the free exciton emission intensity should be proportional to the concentration of free electrons, which, according to our model, abruptly decreases when the temperature reaches T^* (Fig. 8). To illustrate that the exciton emission behavior supports our model, we will derive below an expression for the free exciton emission intensity and compare its temperature dependence with the experimental data.

From Eq. (A4) of Appendix A, within a commonly used approach,[28–32] we can obtain the following expression for the integrated emission intensity related to free excitons

$$\eta_x = \frac{N_x}{\tau_x G} = \frac{C_x np/G}{1 + \tau_x Q_x}, \tag{29}$$

where N_x and $\tau_x = \mathcal{K}T^{3/2}$ are the concentration and lifetime of free excitons. $\mathcal{K}$ is a constant of the order of 10^{-12} s/K$^{3/2}$ (Ref. 31), and $Q_x = 0.5C_xN_{cv}\exp(-E_x/kT)$, where $N_{cv} = 2(2\pi m_x kT)^{3/2}/h^3$ is the density of states for free excitons with mass m_x (Refs. 31 and 32). The dashed red curve in Fig. 8 shows a fit of Eq. (29) with $E_x = 33$ meV and other parameters given in the figure caption. According to Eq. (29), the decrease of the free exciton emission intensity with increasing temperature from ∼50 to ∼150 K is caused by the increase of Q_x and τ_x, and this decrease is partially compensated by an increase in n with temperature. The value of E_x in this fit is larger than the value $E_x = 26$ meV obtained for high-quality GaN from the exciton PL spectroscopy.[33] This indicates that we apparently overestimated the value of E_D for the shallow donor in GaN. Indeed, due to the relatively high concentrations of donors and acceptors, the effective value of E_D in Zn-doped GaN should be smaller than in high-quality undoped GaN. In fact, the temperature dependence of the quantum efficiency of the BL band calculated with Eqs. (7)–(12) is quite insensitive to the variation of E_D in the range from 5 to 50 meV.

V. DISCUSSION

A. Early reports on PL quenching in other materials

Indications of tunable PL quenching were reported in studies of phosphors beginning in the 1940's. Klasens[34] and Vergunas and Gavrilov[35] observed a gradual PL quenching from defects in ZnS that started at a characteristic temperature, and that temperature shifted to larger values with increasing excitation intensity. A similar shift was observed with decreasing concentrations of nonradiative defects (then called "killer centers") in ZnS.[34] Both observations are consistent with the shift of T^* with G given in Eq. (22) of our model. At the time, these researchers interpreted this temperature dependence using Eq. (1) by suggesting that the product $\nu\tau$ is not constant but depends on excitation intensity as $G^{-1/2}$. Klasens,[36] Garlick and Gibson,[37] and Bube[38] used $\nu\tau \propto G^{1-n}$, where n varies between 1 and 2, to explain extensive data on PL from defects in ZnS. In all these papers the activation energy E_A in Eq. (1) was identified with the ionization energy of a defect level not far from the valence band. There were no observations of particularly abrupt quenching of PL with increasing temperature, although Klasens[36] suggested that this might be possible. However, this speculation employed a rather poorly justified two-center model consisting of a radiative donor close to the valence band and a nonradiative acceptor close to the conduction band. His model did predict a linear increase of $1/T^*$ with $1/\ln G$, but, beyond the drop, the PL intensity was predicted to decrease as $\exp(E_A/2kT)$ with increasing temperature.

Later, Maeda[39] observed tunable quenching of PL attributed to DAP transitions in GaP. In his experimental data, $1/T^*$ increased with excitation intensity as $1/\ln G$, but the steepest slope in his semilog plot versus inverse temperature was only 118 meV. Maeda[40] also observed tunable although not abrupt quenching of PL in semi-insulating CdS with activation energy as large 140 meV and a shift of T^* with excitation intensity in both PL and photoconductivity and *only in high-resistivity* CdS. These observations appear consistent with our model, which predicts both a drop in PL and a decrease in conduction electron density n at T^*. This last report is the most recent mention of tunable quenching in PL of which we are aware.

B. Abrupt tunable quenching of PL in high-resistivity Zn-doped GaN

We observed an abrupt tunable thermal quenching of PL in high-resistivity Zn-doped GaN. The BL band intensity drops sharply at a crossover temperature T^*, the value of which strongly depends on excitation intensity. This drop is much steeper than is seen at comparable temperatures in n-type GaN, and the PL quantum efficiency η decreases by several orders of magnitude over an interval ∼10 K.

These observations of abrupt thermal quenching of PL are consistent with a rate-equation model that is presented in detail in Sec. IV. This model, in its basic form, supposes that the samples are high-resistivity p type and contain three major defect species. The numerical solutions of the rate-equation model proposed in Sec. IV to describe high-resistivity GaN agree well with the experimental observations, as can be seen in Fig. 6, and the parameters needed are reasonable and are consistent with the information that we could obtain from other sources. The model allows us to identify the crucial small parameter ζ defined in Eq. (25). As Eqs. (27) and (28) show, the smaller the parameter ζ, the greater the drop and the steeper the slope of the quenching on the semilog plot.

The model not only explains the position and steepness of the slope for any given sample, but also accounts for the dependence of the temperature of the abrupt quenching on the generation rate G. This can be seen in Fig. 7. The characteristic temperature of the quenching T_0 represents a temperature at which the constant low-temperature value of the quantum efficiency, when extrapolated to higher temperatures, crosses the largest slope of the dependence in its quenching region. In Sec. IV we defined the characteristic temperature of the quenching T^* more physically motivated as the temperature at which the system crosses over from one simple, approximate, type of behavior to another, in which different terms in the rate equations dominate, as discussed in Appendix B. The difference between $1/T_0$ and $1/T^*$ is small (about 3×10^{-4} K^{-1} for sample ap269) and is independent of the excitation intensity. Thus, the use of $1/T_0$ instead of $1/T^*$ will cause an overestimate of parameter B (by about a factor of 4 for sample ap269). However, the use of both $1/T_0$ and $1/T^*$ gives the same slope in their dependence on $\ln G$, and this slope can be used to determine the activation energy E_A of the acceptor in our model. It is easier to find T_0 from a graph such as seen in Fig. 5 since finding T^* requires performing a precise fit similar to the one in Fig. 6. The fit in Fig. 7 allows us not only to find E_A, but also to find the parameter B and then to estimate $N_A - N_D$ from Eq. (23). By using data in Fig. 7 and the value of η_0 for the BL band from Table I, we find that the value of $N_A - N_D$ for all high-resistivity GaN:Zn samples lies in the range from 2×10^{17} (for sample ap274) to 5×10^{18} (for sample s452). Note that these values would be smaller by approximately a factor of 4 if we used the more accurate value $1/T^*$ instead of the rough value $1/T_0$.

Our model also explains the sudden quenching of the exciton luminescence simultaneously with the sharp quenching of the BL band (Fig. 8). This happens due to the abrupt drop of the free electron concentration at $T \approx T^*$. These results predict that under UV illumination the samples are conductive n type at temperatures below T^* and become p type or high-resistivity n type at higher temperatures. The model also predicts that intensities of other defect-related PL bands caused by transitions of electrons from the conduction band or from the shallow donor should also drop at T^* because, similar to the Zn_{Ga}-related BL band, they depend on the concentrations of free electrons and of electrons bound to shallow donors in a high-resistivity semiconductor. Remarkably, in samples where the PL spectrum contained other PL bands, we observed their quenching at T^* with a large activation energy.

Although the abrupt tunable quenching of PL, discovered and explained in this work, may be observed in high-resistivity semiconductors with n- and p-type conductivity, the experimental dependences shown in Figs. 5 and 6 indicate that at least some GaN:Zn samples are p type. The BL band, weakly dependent on temperature, could be clearly observed in several samples well above T^* when the sensitivity of our PL setup allowed for reliable detection of PL. In the case of high-resistivity n-type GaN:Zn we expect to see quenching with an activation energy close to 0.4 eV immediately after the abrupt transition, as shown in Fig. 14. The results of this work show that PL can be used as contactless method for distinguishing p- and n-type conductivity in high-resistivity semiconductors in which abrupt quenching of PL is observed.

C. Nonradiative defects in GaN

Calculations based on density-functional theory predict formation of donors in GaN doped with acceptors.[41] The main candidate is nitrogen vacancy V_N which is expected to exist in several charge states and most probably is a negative-U defect.[41,42] V_N has a low formation energy in p-type GaN and a relatively high diffusion probability when in the 3+ state.[43] In this work we considered a simple deep donor as the nonradiative S center. However, the behavior of PL in GaN containing multicharged nonradiative donors is expected to be similar because for the conditions of PL at low temperature the multicharged nonradiative donor will be saturated with electrons and will appear only in two charge states, + and 0. The details of thermal quenching of PL for the case of the multicharged nonradiative defects were beyond the scope of the present paper. Based on results of this work, we can predict some properties of the unknown nonradiative defect in GaN. It should be a deep donor (deeper than 0.4 eV), with a concentration of 10^{17}–10^{18} cm^{-3} in Zn-doped GaN. It has large capture cross sections for both electrons and holes (the electron-capture coefficient for its S^+ state and the hole-capture coefficient for its S^0 state are of the order of 10^{-7}–10^{-6} cm^3/s).

We expect that during high-temperature growth V_N is mobile and forms complexes with hydrogen,[44] Zn_{Ga}, and other acceptors. To the best of our knowledge, the properties of a complex such as V_NZn_{Ga}, which is expected to be a doubly charged donor, have not been investigated theoretically. Therefore, the formation energy and energy levels of this complex are unknown.

An obvious question is whether the tunable abrupt quenching of PL found in Zn-doped GaN could also be seen in Mg-doped GaN. Magnesium is the only impurity currently available for reliable production of p-type GaN. In GaN heavily doped with Mg ($N_{Mg} > 10^{18}$ cm^{-3}) a broad blue band dominates in the PL spectrum. The blue band has a maximum that shifts from ~2.7 to 2.9 eV with increasing excitation intensity, and this band is attributed to DAP-type transitions involving a deep donor ($E_D \approx 0.4$ eV) and the shallow Mg_{Ga} acceptor ($E_A \approx 0.15$–0.20 eV) (Ref. 45). The DAP transitions involving the deep donor become dominant in PL from GaN:Mg due to the large concentration of Mg acceptors and the relatively large size of the hole wave function for the shallow acceptors. The deep donor is assumed to be the V_NMg_{Ga} complex.[46] The intensity of the blue band in Mg-doped GaN does not change much with temperature, and no abrupt or tunable quenching of PL has been reported for this material.[8] If the same nonradiative donor, as in GaN:Zn, caused the inverse population of energy levels and was the bottleneck in recombination of electrons in GaN:Mg, we would expect, according to numerical calculations, a small (by a factor of 10 at most) and not abrupt drop of the blue band at temperatures around 100 K. This is because the value of the drop decreases with decreasing T^* and with increasing E_D, see Eq. (27). Moreover, the expected drop may be considerably rounded due to large potential fluctuations typical for GaN:Mg (Ref. 45).

It appears that GaN doped with Zn, moderately contaminated with oxygen, and containing a deep nonradiative donor due to self-compensation, is an especially favorable material for the observation of the abrupt and tunable thermal quenching of PL. Apparently this material is not appreciably contaminated with other defects and has moderate potential fluctuations. Relatively intense exciton emission containing sharp lines in these samples (at low temperature and sufficiently high excitation intensity) supports the latter assumption.

VI. SUMMARY

We observed dramatic thermal quenching of the blue luminescence band in Zn-doped GaN layers. Namely the PL intensity abruptly decreases at a characteristic temperature T^*, the value of which strongly depends on excitation intensity. The phenomenon has been explained within a phenomenological model, with the assumption that the samples are either high-resistivity n type or p type and contain three major species: an acceptor Zn_{Ga}, a shallow donor O_N, and an unknown nonradiative deep donor. It is possible that the deep donor is the anticipated nitrogen vacancy V_N or the V_NZn_{Ga} complex in p-type GaN. In this work we also suggested a method of how from the study of PL one can determine the type of conductivity in semi-insulating semiconductors when it is difficult to determine it by electrical methods.

ACKNOWLEDGMENTS

The authors are grateful to H. Morkoç from Virginia Commonwealth University who provided GaN samples svt750

and r6623 and R. Molnar from MIT Lincoln Lab for GaN:Zn samples 1393 and 1394. A.A.K. is grateful to VCU's International Partnership Universities Initiative program. M.F.B. and T.M. would like to thank Arthur and Ellen Bishop and Bishop Orchards for providing computational facilities.

APPENDIX A: CALIBRATION OF THE QUANTUM EFFICIENCY

A calibration of the optical setup is necessary to obtain a reasonable estimate of the absolute internal quantum efficiency of PL. The method of determination of the internal quantum efficiency from the temperature dependence of PL was suggested in Refs. 47 and 13 and will be described below in more detail. The main idea of the method can be formulated as follows: The thermal quenching of one of the radiative recombination channels results in the simultaneous increase of recombination rate (or PL intensity) via all other recombination channels, and the magnitude of this relative increase depends on the absolute internal quantum efficiency of the quenching channel. If one can determine the absolute internal quantum efficiency for one "calibration" sample, then the internal quantum efficiency of different PL bands for other samples can be estimated by comparing the integrated PL intensities, provided that all the samples are measured under identical conditions.

An analogy to the method of calibration of quantum efficiency can be found in the determination of the magnitude of the current in a parallel resistor network in which resistances are unknown and the total current I is held constant. Suppose that there is a switch in each branch that can be opened to cut off the current through that branch. The switches are opened one at a time, while one monitors the current in a branch for which the switch remains closed. One then records the ratio R_k between the current with k switches closed to that with $k-1$ switches closed, $R_k = I_k/I_{k-1}$. The initial current I through the network can then be found, for $k = 0,1,2,\ldots,$ from the ratios R_k. In the PL experiment, the generation rate G plays the role of the constant current source, and the recombination currents play the role of the currents through the individual resistors. Thermal quenching of the electron recombination currents sometimes produces clear steps in temperature dependences of PL intensity.[13,47,48] The latter process can be modeled with rate equations that permit the current steps to be extrapolated back to low temperature, and that is what we do in our calibration procedure described below.

To estimate the internal quantum efficiency of PL bands in this work, we have used as a calibration standard a degenerate n-type Si-doped GaN sample r6623 grown by MBE. This sample, having a free-electron concentration of about $n \approx 3 \times 10^{18}$ cm^{-3} and a relatively high concentration of unidentified shallow acceptors, demonstrated an exceptionally high quantum efficiency for the UVL band at low temperature.[48] Si-doped GaN contains shallow donors D with concentration N_D, several acceptors A with concentrations $N_{A\alpha}$, and nonradiative centers S with concentration N_S. In the sample r6623, chosen as a calibration standard, the equilibrium concentration of free electrons is far larger than the concentration of photogenerated electrons at any temperature. Essentially all acceptors are ionized, and there are no free holes in the valence band in the dark.

Under continuous illumination, electron-hole pairs are produced with a generation rate G per unit volume, and this produces a free hole concentration p, with a negligible increase in free electron concentration n. Holes are then captured by acceptors at a rate $C_{pA\alpha}N^-_{A\alpha}p$, where $C_{pA\alpha}$ is the hole-capture coefficient for the αth acceptor and $N^-_{A\alpha}$ is the concentration of negatively charged acceptors. Competing with this is the formation of excitons of steady-state concentration N_x with the rate $C_x np$, where C_x is the exciton formation coefficient. Also competing is the nonradiative recombination of electrons and holes, which has the rate $C_{pS}N^-_S p$, where C_{pS} and N^-_S are the hole-capture coefficient and concentration of nonradiative centers, respectively. For all these cases, holes captured by defects or excitons may return to the valence band as a result of thermal excitation. The rate of these processes is Q_i, which is proportional to $\exp(-E_i/kT)$, where E_i is the binding energy of the acceptors, nonradiative defects, or excitons. The rate of change of the free hole concentration in the valence band is then given by

$$\frac{dp}{dt} = G - \sum_\alpha C_{pA_\alpha}N^-_{A_\alpha}p - C_{pS}N^-_S p + \sum_\alpha Q_{A_\alpha}N^0_{A_\alpha} + Q_S N^0_S - C_x np + Q_x N_x = 0. \quad \text{(A1)}$$

The rates of change of concentration of neutral acceptors, nonradiative centers, and excitons are then given by

$$\frac{dN^0_{A_\alpha}}{dt} = C_{pA_\alpha}N^-_{A_\alpha}p - C_{nA_\alpha}N^0_{A_\alpha}n - Q_A N^0_{A_\alpha} = 0, \quad \text{(A2)}$$

$$\frac{dN^0_S}{dt} = C_{pS}N^-_S p - C_{nS}N^0_S n - Q_S N^0_S = 0, \quad \text{(A3)}$$

$$\frac{dN_x}{dt} = C_x np - \frac{N_x}{\tau_x} - Q_x N_x = 0, \quad \text{(A4)}$$

respectively.

Since the free electron concentration is approximately constant in these rate equations, we can define inverse relaxation times $\tau^{-1}_{A_\alpha} = C_{nA_\alpha}n$ and $\tau^{-1}_S = C_{nS}n$, where C_{nA_α} and C_{nS} are the electron capture coefficients for the αth acceptor and the nonradiative center. Because the sample is degenerate, shallow donors are almost completely ionized, and so do not contribute to the recombination currents. The transitions that occur are shown schematically in Fig. 17. To simplify the notation, in the first term on the right-hand side in Eqs. (A2)–(A4), we let C_i represent C_{pA_α}, C_{pS}, and C_x, and we let N^-_i represent $N^-_{A_\alpha}$, N^-_S, and n. In the second and third terms, we let N^0_i represent $N^0_{A_\alpha}$, N^0_S and N_x. Using this compact notation, with N recombination channels, then the rate of change of the concentration of holes p in the valence band is given by

$$\frac{dp}{dt} = G - \sum_{i=1}^{N} C_i N^-_i p + \sum_{i=1}^{N} Q_i N^0_i = 0. \quad \text{(A5)}$$

The corresponding rate of change of the neutral species N^0_i is

$$\frac{dN^0_i}{dt} = C_i N^-_i p - \frac{N^0_i}{\tau_i} - Q_i N^0_i = 0. \quad \text{(A6)}$$

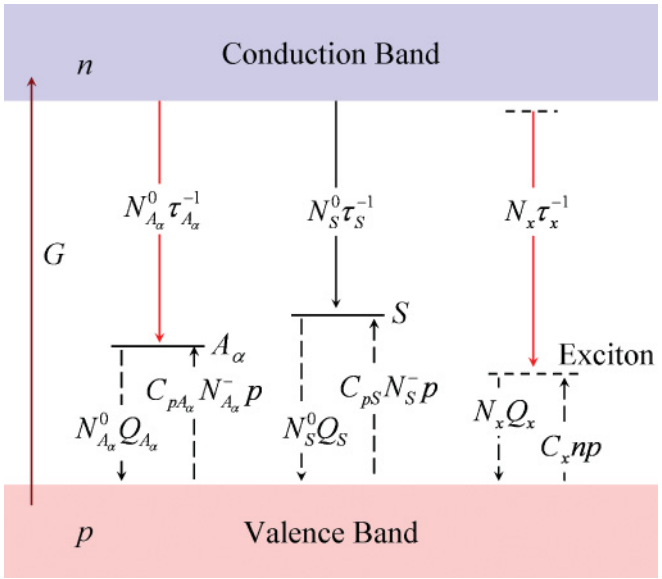

FIG. 17. (Color online) Energy level diagram showing the model used for evaluation of the absolute internal quantum efficiency of PL in the calibration sample. Vertical solid lines indicate transitions for electrons, dashed lines transitions for holes. Energy levels for the exciton, shown with dashed lines, are not real.

One expression for the low-temperature quantum efficiency η_{i0} of channel i is given by $C_i N_i^- p/G$. Since $Q_i \approx 0$ at low temperature, we can see from Eq. (A5) that G is then equal to the sum of this quantity over all channels, and the low-temperature quantum efficiency, η_{i0} becomes,[49]

$$\eta_{i0} = \frac{C_i N_i^- p}{\sum_{j=1}^N C_j N_j^- p} = \frac{C_i N_i^-}{\sum_{j=1}^N C_j N_j^-}. \tag{A7}$$

The quantum efficiency is related to the PL intensity of the ith radiative channel, which can be written as N_i^0/τ_i (which is the same as $G\eta_{i0}$ at low temperature). We first solve for p from Eq. (A5), and rewrite the result in terms of η_{i0} from Eq. (A7) to obtain

$$p = \frac{\eta_{i0}}{C_i N_i^-}\left(G + \sum_{j=1}^N Q_j N_j^0\right). \tag{A8}$$

We substitute this into Eq. (A6) and solve for $Q_i N_i^0$, yielding

$$Q_i N_i^0 = \gamma_i (G + \zeta), \tag{A9}$$

where

$$\gamma_i = \frac{\tau_i Q_i}{1 + \tau_i Q_i}\eta_{i0}, \tag{A10}$$

and

$$\zeta = \sum_{j=1}^N Q_j N_j^0. \tag{A11}$$

We now sum Eq. (A9) over all i, which now gives us an additional ζ on the left-hand side of the equation, so that Eq. (A9) becomes simply

$$\zeta = (G + \zeta)\gamma, \tag{A12}$$

where

$$\gamma = \sum_{j=1}^N \gamma_j. \tag{A13}$$

We solve this equation for ζ to obtain

$$\zeta = \frac{\gamma}{(1-\gamma)}G. \tag{A14}$$

We can substitute this back into Eq. (A9) to obtain an expression for the bound hole concentration for species i.

$$N_i^0 = \frac{\gamma_i}{Q_i(1-\gamma)}G. \tag{A15}$$

It is now useful to define the quantity η_i^*, which we will see later is the quantum efficiency of the ith channel at a temperature just below its quenching temperature,[49]

$$\eta_i^* = \eta_{i0}(1 - \gamma + \gamma_i)^{-1}. \tag{A16}$$

We now use Eq. (A10) to replace γ_i in Eq. (A16), and this enables us to write $(1-\gamma)^{-1}$ in terms of η_i^* as

$$(1-\gamma)^{-1} = \frac{\eta_i^*(1 + \tau_i Q_i)}{\eta_{i0}[1 + \tau_i Q_i(1 - \eta_i^*)]}. \tag{A17}$$

Then N_i^0 in Eq. (A15) can be written in terms of η_i^* as

$$N_i^0 = \frac{\tau_i G \eta_i^*}{1 + \tau_i Q_i(1 - \eta_i^*)}. \tag{A18}$$

We will use this to write the quantum efficiency of the ith recombination channel as

$$\eta_i(T) = \frac{N_i^0}{G\tau_i} = \frac{\eta_i^*}{1 + \tau_i Q_i(1 - \eta_i^*)}, \tag{A19}$$

which is the same as Eq. (5) in Ref. 13. The characteristic temperature of the quenching of the ith channel T_i can be found from condition

$$\tau_i Q_i(1 - \eta_i^*) = 1. \tag{A20}$$

Since $\tau_i Q_i$ is negligible compared with unity at $T < T_i$, the quantity η_i^* is the quantum efficiency of the ith channel just below its quenching temperature.

According to Eq. (A19), the quenching of any PL band (or a nonradiative channel) should result in simultaneous (and equal) stepwise increase in intensities of all other PL bands, which is the manifestation of a competition for minority carriers. The higher the quantum efficiency of a PL band, the larger will be a rise of all other PL bands after its quenching. In practice, however, observations of such steps in temperature dependences of PL bands and their correct interpretation are very rare. This is because usually the quantum efficiency of PL is very low, and small steps are difficult to detect. Moreover, η_{i0} in the expression for η_i^* may not be a constant because capture coefficients C_i may depend on temperature. This will result in a temperature dependence of η_i^* not related to quenching. Then, a rise of η_i^* due to a rise in η_{i0} may be confused with a step caused by quenching of some channel in this temperature region.

However, for some samples, very clear steps in temperature dependences of PL bands were observed that could be fit well by Eq. (A19) with constant or slowly changing parameters η_{i0} (Refs. 13,47, and 48). Such samples can be used for the

calibration of the internal quantum efficiency. It is preferred that one PL band (k) in a calibration sample has a very high quantum efficiency and a weak or, even better, no dependence of τ_k on temperature, while other PL bands (i) have orders of magnitude lower but detectable intensities. In our calibration sample r6623, the low-temperature integrated intensity of the UVL band exceeds those of the exciton and YL bands by at least two orders of magnitude, and the intensity of the UVL band is exceptionally high when compared to any PL band in any other GaN sample we have analyzed in the past decade. The temperature dependences of the integrated PL intensities are shown in Fig. 18 in relative units (right axis). Note that, although this figure is similar to Fig. 2 in Ref. 48, these are new experimental data and new fits to the data. Remarkably, after five years of storing the sample in ambient conditions, no significant degradation or any other changes in PL could be noticed. For this sample, by using an approximation $\eta_i^* \ll \eta_k^* < 1$, the following expressions could be readily derived from Eq. (A19) for the exciton and YL bands, both denoted with index i, and for the UVL band denoted with index k:

$$\eta_i(T) \approx \frac{\eta_i^*}{1+\tau_i Q_i}, \tag{A21}$$

with

$$\eta_i^* \approx \frac{\eta_{i0}}{1-\eta_k(0)\frac{\tau_k Q_k}{1+\tau_k Q_k}}, \tag{A22}$$

and

$$\eta_k(T) \approx \frac{\eta_k(0)}{1+\tau_k Q_k[1-\eta_k(0)]}. \tag{A23}$$

In these expressions we replaced η_{k0} with its value $\eta_k(0)$ at low-temperature because the quantum efficiency of the UVL band is temperature independent at temperatures below its quenching.

The thermal quenching of the UVL band begins at ~120 K (Fig. 18). But below this temperature the quantum efficiencies of the exciton and YL bands η_i^* already vary slowly with increasing temperature for different reasons (thermal quenching of the exciton emission and apparent small variation of the coefficients C_i). These slowly varying dependences of the exciton and YL intensities (or η_{i0}) can be extrapolated to higher temperatures as if they were not affected by the thermal quenching of the UVL band (by forcing $Q_k = 0$). We denote such extrapolated dependences by $\eta_{i0}(T)$ and show them as dashed curves in Fig. 18. Instead of describing these dependences with expressions of the form

$$\eta_{i0}(T) = \frac{\eta_{i0}}{1+\tau_i Q_i}, \tag{A24}$$

that can be obtained from Eqs. (A22) and (A23) with $Q_k = 0$, and which do not account for variation of C_i with temperature, we will formally fit them with the commonly used expression[50]

$$\eta_{i0}(T) = \frac{\eta_i(0)}{1+A_1 e^{-(E_1/kT)}+A_2 e^{-(E_2/kT)}}, \tag{A25}$$

where $\eta_i(0)$ is the quantum efficiency of the ith channel at zero (or lowest) temperature, and constants A_1, A_2, E_1, and E_2 are fitting parameters, which may have no physical meaning. We fit Eq. (A25) to the experimental data in the region below

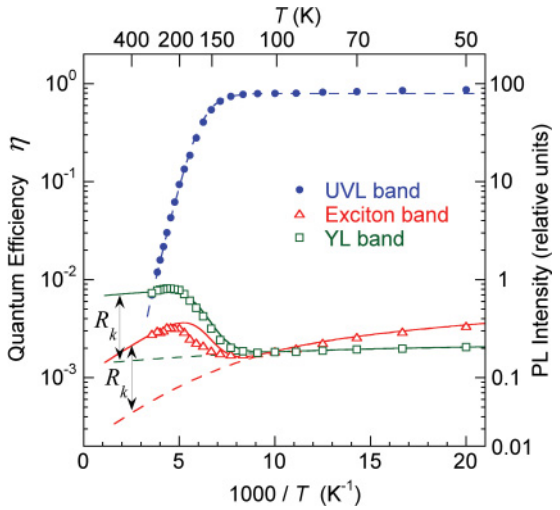

FIG. 18. (Color online) Temperature dependence of the absolute internal quantum efficiency (left axis) and integrated PL intensity in relative units (right axis) for the UVL, exciton, and YL bands in Si-doped GaN sample r6623. $P_{exc} = 3 \times 10^{-4}$ W/cm^2. Dashed curves are fit with Eq. (A24) with the following parameters: $\eta_{YL}(0) = 2.16 \times 10^{-3}$, $A_1 = 0.6$, $A_2 = 0$, and $E_1 = 10$ meV for the YL band; $\eta_x(0) = 1.45 \times 10^{-2}$, $A_1 = 8$, $A_2 = 60$, $E_1 = 4$ meV, and $E_2 = 30$ meV for the exciton band; $\eta_{UVL}(0) = 0.80$, $A_1 = 5.4T^{3/2}$, $A_2 = 0$, and $E_1 = 130$ meV for the UVL band. Solid curves are calculated with Eq. (A27) for the YL and exciton bands, both with $\eta_k(0) = 0.80$.

the quenching of the UVL band and extrapolate it to higher temperatures (dashed lines in Fig. 18).

Now, accounting for the quenching of the UVL band (kth channel), the "real" dependences $\eta_i(T)$ can be expressed from Eqs. (A21), (A22), and (A24) as

$$\eta_i(T) = \eta_{i0}(T)\left(1-\eta_k(0)\frac{\tau_k Q_k}{1+\tau_k Q_k}\right)^{-1}. \tag{A26}$$

Finally, from Eqs. (A23) and (A26), by eliminating $\tau_k Q_k$, we arrive at

$$\eta_i(T) = \eta_{i0}(T)\frac{1-\eta_k(T)}{1-\eta_k(0)}, \tag{A27}$$

or

$$\frac{I_i^{PL}(T)}{I_{i0}^{PL}(T)} = \frac{\eta_i(T)}{\eta_{i0}(T)} = \frac{1-\frac{I_k^{PL}(T)}{I_k^{PL}(0)}\eta_k(0)}{1-\eta_k(0)}, \tag{A28}$$

where the $I_k^{PL}(T)/I_k^{PL}(0)$ can be found from fitting experimental data for the UVL band with Eq. (A25). The only parameter that was determined in the fitting of Eq. (A28) to the "real" temperature dependences of PL from all ith channels is $\eta_k(0)$. In Fig. 18 the experimental data for the YL and exciton bands are fitted by Eq. (A28) (solid curves) with $\eta_k(0) = 0.80$ for both. Now the relative PL intensities scale (right axis in Fig. 18) can be converted to the absolute internal quantum efficiency scale (left axis). This fit and the value of $\eta_k(0)$ are in excellent agreement with our old data for the same sample.[48] The fact that both the YL and exciton bands increase by the same value during the quenching of the UVL band [or require the same $\eta_k(0)$ to fit their temperature dependences] indicates that the

stepwise rise of these bands is not accidental and is adequately described by our model.

When the quenching regions for different channels do not overlap, and the temperature dependence of η_{i0} is negligible [i.e., $\eta_{i0} = \eta_i(0)$], it is possible to calibrate the system much more simply and quickly, and with almost the same accuracy, by a calculation that is similar to the parallel resistor analogy mentioned earlier. Suppose that we number the channels in increasing order of quenching temperature, so that the first channel to be quenched is $j = 1$. Then the quantity $\tau_j Q_j$ is much less than unity before channel j quenches and is much greater than unity after it quenches. Since the quantum efficiency of all channels added together must be unity, when a channel k quenches, then it is clear that the quantum efficiency must be redistributed to all the channels that have not yet quenched. Therefore, if the kth channel quenched before the ith channel, we need to determine the effect of its quenching on PL intensity of the arbitrary ith channel. Therefore, the PL of the radiative ith channel will be affected by the quenching of all channels that quench at lower temperatures than it does. In practice, the nonradiative channels often quench at much higher temperatures than the radiative channels of interest, and therefore in what follows, the quenched channels will be assumed to be radiative ones.

Suppose that at a particular temperature T_k all the channels for $j < k$ have already quenched, and the channel $j = k$ is in the process of quenching. Therefore, from Eq. (A10), for $j < k$, $\tau_i Q_i \gg 1$ and $\gamma_i \approx \eta_i(0)$. For $j > k$, $\tau_i Q_i \ll 1$ and $\gamma_i \approx 0$. Therefore, using Eq. (A19) for a radiative channel with $i > k$, the intensity in the vicinity of the quenching temperature for channel k can be written as

$$I_i^{\mathrm{PL}} = G\eta_i(0)\left(1 - \sum_{j\neq i,\, j=1}^{N} \eta_j(0) - \gamma_k\right)^{-1}. \tag{A29}$$

Since $\gamma_k \approx \eta_k(0)$ before channel k quenches and zero after, the ratio $R_{i,k}$ of the intensity of channel i before the quenching of channel k to that after its quenching is given by

$$R_{i,k} = R_k = \frac{I_i^{\mathrm{PL}}(T > T_k)}{I_i^{\mathrm{PL}}(T < T_k)} = \frac{1 - \sum_{j=1}^{k-1}\eta_j(0)}{1 - \sum_{j=1}^{k}\eta_j(0)}. \tag{A30}$$

Note that the right-hand side of this equation does not depend on i, and so this must be the same for all channels that have not yet quenched. This can be written in a more transparent way as

$$R_k = 1 + \frac{\eta_k(0)}{1 - \sum_{j=1}^{k}\eta_j(0)}, \tag{A31}$$

where now it can be seen that $R_k > 1$ since the second term on the right must be positive. Using $I_j^{\mathrm{PL}}(0) = G\eta_j(0)$, we can rewrite this as

$$\frac{1}{R_k - 1} = \frac{1}{\eta_k(0)} - \frac{\sum_{j=1}^{k} I_j^{\mathrm{PL}}(0)}{I_k^{\mathrm{PL}}(0)}. \tag{A32}$$

Solving for $\eta_k(0)$, we have

$$\eta_k(0) = \left(\frac{1}{R_k - 1} + \frac{\sum_{j=1}^{k} I_j^{\mathrm{PL}}(0)}{I_k^{\mathrm{PL}}(0)}\right)^{-1}. \tag{A33}$$

Therefore, using this expression, the quantum efficiency of the kth channel at very low temperature can be found from the step R_k and the measured integrated intensities of all the quenched bands relative to that of the kth channel at low temperature. Equation (A33) is the same as Eq. (13) of Reshchikov and Korotkov,[13] except that in that paper it was erroneously stated that the sum should be taken over all the channels that had been thermally quenched prior to the quenching of the kth band. This is also the same as Eq. (12) of Reshchikov and Morkoc,[8] which also had the erroneous description and had not written that the intensities should all be at low temperature. In Eq. (3) of the conference paper by Reshchikov *et al.*,[48] the formula was rewritten correctly in such a way that the sum over intensities included only bands that quenched prior to the kth channel. It is possible to rewrite this expression as

$$\eta_k(0) = \frac{R_k - 1}{R_k}\left(1 - \sum_{j=1}^{k-1}\eta_j(0)\right). \tag{A34}$$

This equation allows one to obtain a quick estimate of the quantum efficiency of the kth channel. For instance, the first band to quench would yield

$$\eta_1(0) = \frac{R_1 - 1}{R_1}, \tag{A35}$$

so that only the size of the step is needed for an estimate of the quantum efficiency. One could find the quantum efficiency of the second channel by using this together with the second step size R_2 in Eq. (A34), and so on. If the first step is very small compared to the second, then the $\eta_1(0)$ in Eq. (A34) could even be neglected. In our example, $R_k \approx 5$ for the YL band in the region of quenching of the UVL band (Fig. 18). Although the UVL band quenches after the exciton band, the latter can be ignored since its relative intensity is very weak. Then, Eq. (A35) gives $\eta_k(0) \approx 1 - 1/R_k = 0.8$.

This form now makes the analogy with the simple parallel resistor network clear, and one obtains exactly the results given by Eqs. (A34) and (A35) if one defines the quantum efficiency η_{k0} to be the ratio between the current in the kth wire to the constant current source when all the switches are closed (currents in all wires). When one opens the first switch (so that the first wire has zero current), the current in all the other branches increases, and the quantum efficiency of the kth branch is given simply by Eq. (A35). When the other switches are opened successively, then the quantum efficiencies of those branches can be found from Eq. (A34), just as in the PL case.

APPENDIX B: DERIVATION OF APPROXIMATE ANALYTIC SOLUTIONS TO THE MODEL NEAR THE CROSSOVER TEMPERATURE T^*

The way in which the system switches from a deep donor that is almost completely neutral to one that is nearly completely ionized, thereby causing a dramatic decrease in PL over a very small temperature interval, becomes more apparent if we derive approximate analytical solutions in the vicinity of the crossover temperature T^*, that is, in the range 100 K $< T <$ 300 K. In explaining the approximations that we make to get simple analytic results, we will use the

parameter values that correspond to the calculated curves in Fig. 6, choosing the representative value $G = 10^{19}$ cm^{-3}s^{-1}. The analytic solutions apply to the entire range of parameters shown there, and this particular value is simply used to make the discussion more concrete. The derivations are for the high-resistivity p-type case, for which the numerical solutions are shown as the solid curves in Fig. 6.

For high resistivity materials and sufficiently low excitation intensity (such as the excitation intensities in the experiments reported in this paper), the concentrations of free electrons, free holes, and ionized shallow donors are much smaller than other concentrations in the region around the crossover. This means that the fractional concentration N_D^0/N_D of electrons in shallow donors is very small, and so, to a very good approximation, we can write $N_D^+ \approx N_D$. Therefore, from the charge conservation relation of Eq. (12), we have

$$N_A^- \approx N_D + N_S^+, \tag{B1}$$

and

$$N_A^0 \approx N_A - N_D - N_S^+. \tag{B2}$$

To begin, we solve for N_D^0 in Eq. (9) with $N_D^+ \approx N_D$

$$N_D^0 \approx \frac{C_{nD} N_D}{Q_D} \alpha n. \tag{B3}$$

where

$$\alpha = \left(1 + C_{DA} N_A^0 / Q_D\right)^{-1}. \tag{B4}$$

In this expression for α, the quantity $C_{DA} N_A^0/Q_D < C_{DA} N_A/Q_D$ is very small for a high-resistivity p-type semiconductor in this temperature region. At 100 K $C_{DA} N_A/Q_D \approx 0.02$, decreases exponentially with increasing temperature, and falls to less than 0.003 at the crossover. To simplify these equations, we expand α to lowest order in this small quantity as

$$\alpha \approx \left(1 - C_{DA} N_A^0 / Q_D\right). \tag{B5}$$

Next we solve for the free electron concentration n from Eq. (7) to obtain

$$n = \frac{G + Q_D N_D^0}{C_{nS} N_S^+ + C_{nD} N_D + C_{nA} N_A^0}. \tag{B6}$$

When we substitute for N_D^0 from Eq. (B3) into Eq. (B6), n appears on both sides of the equation. Solving that resulting equation for n and using Eq. (B5) yields

$$n \approx \frac{G}{C_{nS}\left(N_S^+ + \zeta N_A^0\right)}, \tag{B7}$$

where ζ is a small dimensionless parameter given by

$$\zeta = \frac{C_{DA} C_{nD}}{C_{nS}} \frac{N_D}{Q_D} + \frac{C_{nA}}{C_{nS}}. \tag{B8}$$

Specifically, ζ is about 0.001 at 100 K, decreases to about 0.0002 at T^*, and continues to decrease above T^*. Note that this relatively simple form for n emerges as a result of the approximate form of α in Eq. (B5).

Next we find an expression for p in terms of n by using Eq. (10), substitute for n from Eq. (B7) and use $N_S^0 = N_S - N_S^+$ to obtain

$$p = \frac{C_{nS} N_S^+ n}{C_{pS} N_S^0} = \frac{N_S^+ G}{C_{pS}(N_S - N_S^+)\left(N_S^+ + \zeta N_A^0\right)}. \tag{B9}$$

We can get a second expression for p from Eq. (8), which is

$$p = \frac{G + Q_A N_A^0}{C_{pS} N_S^0 + C_{pA} N_A^-}. \tag{B10}$$

In Eq. (B10) we substitute $N_S^0 = N_S - N_S^+$, and the expressions for N_A^-, and N_A^0 from Eqs. (B1) and (B2) to obtain

$$p = \frac{G + Q_A(N_A - N_D) - Q_A N_S^+}{(C_{pS} N_S + C_{pA} N_D) + (C_{pA} - C_{pS}) N_S^+}. \tag{B11}$$

Then we equate the two expressions for p from Eqs. (B9) and (B11) and obtain a cubic polynomial in N_S^+ in which the term $(N_S^+)^3$ has a factor of $(1 - \zeta)$. We divide all terms by $(1 - \zeta)$ and then expand the resulting coefficients to first order in ζ. This leads to a cubic equation in N_S^+, given by

$$(N_S^+)^3 + a(N_S^+)^2 + b N_S^+ + c = 0, \tag{B12}$$

where

$$a = -(N_2 + N_A - N_D + N_S) + \zeta\left[N_A - N_D + N_2\left(\frac{C_{pS}}{C_{pA}} - 1\right)\right], \tag{B13}$$

$$b = [(N_A - N_D)N_S - N_2 N_D] - \zeta[(N_A - N_D)(N_A - N_D + N_S) + N_2 N_D + N_2 \frac{C_{pS}}{C_{pA}}(N_A - N_D + N_S)], \tag{B14}$$

$$c = \zeta N_S (N_A - N_D)\left(N_2 \frac{C_{pS}}{C_{pA}} + N_A - N_D\right), \tag{B15}$$

and

$$N_2 = \frac{G C_{pA}}{Q_A C_{pS}}. \tag{B16}$$

Only one root of this cubic equation satisfies the physical condition that $0 \leqslant N_S^+ \leqslant N_S$. It was the approximation for α in Eq. (B5) that enabled us to reduce the problem to a cubic equation.

Once N_S^+ is determined, we can find N_A^- and N_A^0 by using Eqs. (B1) and (B2). Then, n and p can be obtained from Eqs. (B7) and (B11), respectively. N_D^0 can be found from Eq. (B3), in which we will take $\alpha \approx 1$ or

$$N_D^0 \approx n \frac{C_{nD} N_D}{Q_D}. \tag{B17}$$

The quantum efficiency is then given simply by Eq. (13), which becomes in the above approximation

$$\eta = \left(C_{nA} n + C_{DA} N_D^0\right) N_A^0 \approx \frac{\zeta(N_A - N_D - N_S^+)}{N_S^+(1 - \zeta) + \zeta(N_A - N_D)}. \tag{B18}$$

The solution agrees well with the numerical solution from about 100 to 300 K, and so reliably describes the region of the crossover, as shown in Fig. 12, where the curve calculated

with Eq. (B18) with N_S^+ from the solution of the cubic equation (B12) is indistinguishable from the numerical solution.

Since the solutions of the cubic equation are sufficiently complex that it is hard to extract their physical content, we now obtain approximate analytic expressions for N_S^+ and η that can be used in different temperature regions and in which the crossover temperature T^* is a special point.

At temperatures above the crossover ($T^* < T < 300$ K), $N_S^+ \approx N_S$ and we can neglect the constant term c in Eq. (B12) because $c \ll (N_S^+)^3$ at these temperatures. Then we can eliminate a factor of N_S^+ and be left with the quadratic equation

$$(N_S^+)^2 + aN_S^+ + b = 0, \tag{B19}$$

which has the (physical) solution

$$N_S^+ = -\frac{a}{2} + \sqrt{\left(\frac{a}{2}\right)^2 - b}. \tag{B20}$$

This solution works quite well for temperatures starting about 1 K above T^* up to around 300 K, where the free hole concentration starts to become important in the charge conservation condition of Eq. (12). However, at the temperature we will call T^*, the coefficient b becomes zero, and, in this approximation, N_S^+ drops to zero, becoming negative at lower temperatures. This point occurs for $N_2 = N_2^*$, where

$$N_2^* = N_S(N_A/N_D - 1). \tag{B21}$$

Solving for the temperature using Eqs. (6), (B16), and (B21) produces what we call the crossover temperature

$$T^* = \frac{E_A/k}{\ln(B/G)}, \tag{B22}$$

where

$$B = \frac{C_{pS}N_S(N_A - N_D)N_v}{gN_D}. \tag{B23}$$

Of course, when $c \neq 0$ is included, N_S^+ never goes negative, but the point at T^* is still special since the coefficient b of Eq. (B14) in the polynomial of Eq. (B12) drops dramatically in magnitude because the large concentrations in its expression have canceled, leaving only the term proportional to ζ, which is orders of magnitude smaller. It is the coefficient c, Eq. (B15), which is proportional to ζ that prevents the disaster.

Simple analytical expressions for the case of $T > T^*$ can be obtained if we leave out terms proportional to ζ in the denominator of the quantum efficiency η in Eq. (B18), and this produces

$$\eta \approx \zeta \frac{(N_A - N_D - N_S^+)}{N_S^+}. \tag{B24}$$

An approximate expression for N_S^+ can be obtained from Eq. (B20) by neglecting the terms proportional to ζ in a and b in Eqs. (B13) and (B14)

$$N_S^+ = -\tfrac{1}{2}\sqrt{(N_A - N_D - N_S + N_2)^2 + 4N_2(N_D + N_S)} + \tfrac{1}{2}(N_A - N_D + N_S + N_2), \tag{B25}$$

where N_2 is defined by Eq. (B16). In agreement with experiment, the PL quantum efficiency η in Eq. (B24) can be seen to be very small since it is proportional to the small quantity ζ. The PL quantum efficiency calculated with the approximate formula (B24) for $T > T^*$ is shown in Fig. 12 as the dotted red curve.

Now we will consider the temperature range 100 K to a temperature a couple of degrees above the crossover. In this range, N_S^+ is sufficiently small that the cubic term in Eq. (B12) can be neglected, and we have again a quadratic equation, with the physical solution given by

$$N_S^+ = -\frac{b}{2a} + \sqrt{\left(\frac{b}{2a}\right)^2 - \frac{c}{a}}, \tag{B26}$$

where $(-c/a)$ is positive. The quantum efficiency using this solution is shown in Fig. 12 as the dashed blue curve with squares. At temperatures below the crossover (100 K $< T <$ T^*), $(b/2a)^2 \gg c/a$ and

$$N_S^+ \approx -\frac{c}{b} \approx \frac{\zeta(N_A - N_D)\left(N_A - N_D + \frac{C_{pS}}{C_{pA}}N_2\right)}{N_2N_D/N_S - (N_A - N_D)}. \tag{B27}$$

In the above expression we neglected the term containing ζ in the expression for b taken from Eq. (B14) because it is very small. To obtain an approximate expression for the quantum efficiency η, we start with Eq. (B18), substitute N_S^+ from Eq. (B27), cancel a factor of ζ in the numerator and denominator, and neglect the remaining ζ terms. This yields for the PL quantum efficiency

$$\eta \approx \eta_0\left[1 - \frac{(N_A - N_D)N_S}{N_DN_2}\right], \tag{B28}$$

where

$$\eta_0 = \frac{C_{pA}N_D}{C_{pA}N_D + C_{pS}N_S}. \tag{B29}$$

One of the dramatic features in the data we wish to explain is the steepness of the slope very close to the crossover temperature T^*. Here $(b/2a)^2$ is very small compared with $(-c/a)$, and Eq. (B26) can be reduced to

$$N_S^+ \approx -\frac{b}{2a} + \sqrt{-\frac{c}{a}}. \tag{B30}$$

This approximation is useful for understanding the steepness of the quantum efficiency curve at the crossover temperature.

Right at the crossover, the term $\zeta(N_A - N_D)$ is very small compared with N_S^+, but N_S^+ is small compared with $N_A - N_D$. Therefore, we can write, again very close to the crossover,

$$\eta \approx \zeta\frac{(N_A - N_D)}{N_S^+}, \quad T \approx T^*. \tag{B31}$$

The slope on the semilog plot is given by

$$\frac{d\ln\eta}{d(1/T)} = \frac{1}{\eta}\frac{d\eta}{d(1/T)} \approx -\frac{1}{N_S^+}\frac{dN_S^+}{d(1/T)} = -\frac{d\ln(N_S^+)}{d(1/T)}. \tag{B32}$$

Therefore, the slope of the quantum efficiency η is just the negative of the slope of N_S^+. Thus, we return to the quadratic solution in Eq. (B30). At T^*, the term proportional to ζ in a

[the second term in Eq. (B13)] is small enough to be neglected, and a and c vary slowly compared with b. Also, the term proportional to ζ in b in Eq. (B14) varies slowly compared to the other term. Therefore, the log slope of N_S^+ is simply

$$\left.\frac{d\ln(N_S^+)}{d(1/T)}\right|_{T=T^*} \approx \frac{1}{2aN_S^+}\left.\frac{db}{d(1/T)}\right|_{T=T^*} = \frac{N_D N_2}{2a^* N_S^{+*}}\frac{E_A}{k}, \tag{B33}$$

where superscript $*$ indicates that a given quantity is evaluated at the crossover temperature T^*. Substituting explicit values and using Eq. (B32), we obtain for the log slope of the quantum efficiency to leading order of ζ

$$\frac{d(\ln\eta)}{d(1/T)} \approx \frac{E_A/k}{2\sqrt{\zeta^*\lambda}}, \tag{B34}$$

where ζ^* is from Eq. (B8) evaluated at T^* and

$$\lambda = \left(\frac{N_S}{N_D}\frac{C_{pS}}{C_{pA}} + 1\right)\left[\frac{N_A}{N_D} + \frac{(N_A - N_D)}{N_S}\right]. \tag{B35}$$

Since $\zeta^* \approx 0.0002$ and $\lambda \approx 15.4$, $d(\ln\eta)/d(1/T) \approx 9E_A/k$, which corresponds to the "activation energy" of the slope of about 3.2 eV for $G = 10^{19}\,\mathrm{cm}^{-3}\mathrm{s}^{-1}$ and other parameters as in Fig. 6.

*mreshchi@vcu.edu
†Currently at École Polytechnique Fédérale de Lausanne, Lausanne, Switzerland.
‡Deceased.

[1] H. G. Grimmeiss and H. Koelmans, Naturforsch. **14**, 264 (1959); H. G. Grimmeiss and J. W. Allen, J. Non-Cryst. Solids **352**, 871 (2006).
[2] M. Ilegems, R. Dingle, and R. A. Logan, J. Appl. Phys. **43**, 3797 (1972).
[3] J. I. Pankove, J. E. Berkeyheiser, and E. A. Miller, J. Appl. Phys. **45**, 1280 (1974).
[4] A. L. Vinke, V. G. Sidorov, M. D. Shagalov, Y. K. Shalabutov, and A. N. Vasilishchev, Izvestia Akademii Nauk SSSR. Seria Fizicheskaya **40**, 2338 (1976).
[5] B. Monemar, H. P. Gislason, and O. Lagerstedt, J. Appl. Phys. **51**, 640 (1980).
[6] M. A. Reshchikov, F. Shahedipour, R. Y. Korotkov, M. P. Ulmer, and B. W. Wessels, J. Appl. Phys. **87**, 3351 (2000).
[7] M. A. Reshchikov, H. Morkoç, R. J. Molnar, D. Tsvetkov, and V. Dmitriev, Mater. Res. Soc. Symp. Proc. **743**, L11.1 (2003).
[8] M. A. Reshchikov and H. Morkoç, J. Appl. Phys. **97**, 061301 (2005).
[9] J. I. Pankove, E. A. Miller, D. Richman, and J. E. Berkeyheiser, J. Lumin. **4**, 63 (1971).
[10] E. Ejder and P.-O. Fagerström, J. Phys. Chem. Solids **36**, 289 (1975).
[11] N. I. Kuznetsov, A. E. Nikolaev, A. S. Zubrilov, Y. V. Melnik, and V. A. Dmitriev, Appl. Phys. Lett. **75**, 3138 (1999).
[12] A. Y. Polyakov, A. V. Govorkov, N. B. Smirnov, A. E. Nikolayev, I. P. Nikitina, and V. A. Dmitriev, Sol. St. Electron. **45**, 249 (2001).
[13] M. A. Reshchikov and R. Y. Korotkov, Phys. Rev. B **64**, 115205 (2001).
[14] M. A. Reshchikov, D. Huang, M. Morkoç, and R. J. Molnar, Mater. Res. Soc. Symp. Proc. **693**, I2.10 (2002).
[15] B. I. Shklovskii and A. L. Efros, *Electronic Properties of Doped Semiconductors* (Springer, Berlin, 1984).
[16] D. C. Look, C. E. Stutz, R. J. Molnar, K. Saarinen, and Z. Lilienthal-Weber, Solid State Commun. **117**, 571 (2001).
[17] The temperature-dependent Hall effect data were provided by D. C. Look (Wright State University).
[18] J. F. Muth, J. H. Lee, I. K. Shmagin, R. M. Kolbas, H. C. Casey Jr., B. P. Keller, U. K. Mishra, and S. P. DenBaars, Appl. Phys. Lett. **71**, 2572 (1997).
[19] F. Seitz, Trans. Faraday Soc. **35**, 74 (1939).
[20] R. W. Gurney and N. F. Mott, Trans. Faraday Soc. **35**, 69 (1939).
[21] A. M. Stoneham, *Theory of Defects in Solids* (Clarendon Press, Oxford, 2001).
[22] V. N. Abakumov, V. I. Perel, and I. N. Yassievich, *Nonradiative Recombinations in Semiconductors* (Elsevier, Amsterdam, 1991).
[23] W. Shockley and J. W. T. Read, Phys. Rev. **87**, 835 (1952).
[24] M. A. Reshchikov, Appl. Phys. Lett. **88**, 202104 (2006).
[25] K. Kumakura, T. Makimoto, N. Kobayashi, T. Hashizume, T. Fukui, and H. Hasegawa, Appl. Phys. Lett. **86**, 052105 (2005).
[26] J. Y. Duboz, F. Binet, D. Dolfi, N. Laurent, F. Scholz, J. Off, A. Sohmer, O. Briot, and B. Gil, Mater. Sci. Eng. **50**, 289 (1997).
[27] A. P. Levanyuk and V. V. Osipov, Usp. Fiz. Nauk **133**, 427 (1981); Sov. Phys. Usp. **24**, 187 (1981).
[28] M. D. Sturge, E. Cohen, and K. F. Rodgers, Phys. Rev. B **15**, 3169 (1977).
[29] O. Brandt, J. Ringling, K. H. Ploog, H.-J. Wünsche, and F. Henneberger, Phys. Rev. B **58**, 15977 (1998).
[30] S. Dhar, U. Jahn, O. Brandt, P. Waltereit, and K. H. Ploog, Appl. Phys. Lett. **81**, 673 (2002).
[31] A. Dmitriev and A. Oruzheinikov, J. Appl. Phys. **86**, 3241 (1999).
[32] J. S. Im, A. Moritz, F. Steuber, V. Härle, F. Scholz, and A. Hangleiter, Appl. Phys. Lett. **70**, 631 (1997).
[33] A. V. Rodina, M. Dietrich, A. Göldner, L. Eckey, A. Hoffmann, A. L. Efros, M. Rosen, and B. K. Meyer, Phys. Rev. B **64**, 115204 (2001).
[34] H. A. Klasens, Nature (London) **158**, 306 (1946).
[35] F. I. Vergunas and F. F. Gavrilov, Zh. Exp. Teor. Fiz. **20**, 224 (1950).
[36] H. A. Klasens, J. Phys. Chem. Solids **9**, 185 (1959).
[37] G. F. J. Garlick and F. Gibson, J. Opt. Soc. Am. **39**, 935 (1949).
[38] R. H. Bube, Phys. Rev. **90**, 70 (1953).
[39] K. Maeda, J. Phys. Chem. Solids **26**, 595 (1965).
[40] K. Maeda, J. Phys. Chem. Solids **26**, 1419 (1965).
[41] C. G. Van de Walle and J. Neugebauer, J. Appl. Phys. **95**, 3851 (2004).
[42] M. G. Ganchenkova and R. M. Nieminen, Phys. Rev. Lett. **96**, 196402 (2006).
[43] S. Limpijumnong and C. G. Van de Walle, Phys. Rev. B **69**, 035207 (2004).
[44] B. Szûcs, A. Gali, Z. Hajnal, P. Deak, and C. G. Van de Walle, Phys. Rev. B **68**, 085202 (2003).
[45] M. A. Reshchikov, G.-C. Yi, and B. W. Wessels, Phys. Rev. B **59**, 13176 (1999).

[46]H. Obloh, K. H. Bachem, U. Kaufmann, M. Kunzer, M. Maier, A. Ramakrishnan, and P. Schlotter, J. Cryst. Growth **195**, 270 (1998).

[47]K. D. Glinchuk and A. V. Prokhorovich, Phys. Status Solidi A **44**, 777 (1977).

[48]M. A. Reshchikov, X. Gu, J. Nause, and H. Morkoç, Mater. Res. Soc. Symp. Proc. **892**, FF23.11 (2006).

[49]In general, $\eta_{i0} \neq \eta_i(0)$. While $\eta_i(0)$ is temperature independent, η_{i0} may vary with temperature due to varying capture coefficients C_i, but this does not include any variations due to thermal quenching of other channels, as opposed to η_i^*, where the thermal quenching of other channels is included.

[50]D. Bimberg, M. Sondergeld, and E. Grobe, Phys. Rev. B **4**, 3451 (1971).